NASA Contractor Report 4345

# Improving the Reliability and Modal Stability of High Power 870 nm AlGaAs CSP Laser Diodes for Applications to Free Space Communication Systems

J. C. Connolly, G. A. Alphonse,
D. B. Carlin, and M. Ettenberg

CONTRACT NAS1-18226
MARCH 1991

NASA

NASA Contractor Report 4345

# Improving the Reliability and Modal Stability of High Power 870 nm AlGaAs CSP Laser Diodes for Applications to Free Space Communication Systems

J. C. Connolly, G. A. Alphonse,
D. B. Carlin, and M. Ettenberg
*David Sarnoff Research Center*
*Princeton, New Jersey*

Prepared for
Langley Research Center
under Contract NAS1-18226

NASA
National Aeronautics and
Space Administration
Office of Management
Scientific and Technical
Information Division

**1991**

**Page intentionally left blank**

# PREFACE

This report describes work performed from 19 August 1988 to 1 October 1990 at the David Sarnoff Research Center in the Optoelectronics Research laboratory, M. Ettenberg, Director, under SubContract No. C12187. D. B. Carlin was the Project Supervisor, and J. C. Connolly was the Project Scientist. Other contributors to this research were J. K. Butler, G. A. Evans, G. A. Alphonse, P. D. Gardner, N. A. Dinkel, M. G. Harvey, D. B. Gilbert, T. R. Stewart, K. B. Murphy, D. T. Tarangioli, L. A. DiMarco, D. J. Holmes, and F. Z. Hawrylo.

**Page intentionally left blank**

## TABLE OF CONTENTS

**Page intentionally left blank**

## LIST OF ILLUSTRATIONS

## LIST OF ILLUSTRATIONS (cont.)

## LIST OF ILLUSTRATIONS (cont.)

## LIST OF ILLUSTRATIONS (cont.)

# SUMMARY

The fabrication procedures and theoretical understanding of high-power channeled-substrate-planar (CSP) lasers have been expanded, particularly in areas that focus on increasing the power capability and reliability. The results of this work have been experimentally incorporated into the CSP structure producing laser devices exhibiting extremely low degradation rates at high optical power densities. These results have been obtained without sacrificing the desirable characteristics of the CSP laser, such as beam quality, non-astigmatic wavefronts and modulation performance.

In our work, an improved version of the CSP structure has been demonstrated, the inverse channeled substrate planar (ICSP). This structure is grown by a two-step metalorganic chemical vapor deposition. The structure is a graded index separate confinement-single quantum well (GRIN-SCH) containing a GaAs quantum well with a thickness of 14 nm. This new structure also eliminates the need for a deep zinc diffusion processing procedure to confine electrical carriers to the lasing region. The threshold current for this new CSP laser has been reduced from 70 mA to 15 mA with an increase in overall efficiency. As the performance of the CSP laser has improved, the device reliability has also improved. The results of ICSP lasers placed on room temperature lifetest at 60 mW (50% duty cycle; 100 MHz) have shown degration rates less than 2 mW/Khr, a significant improvement compared with CSP lasers.

A theoretical study examining the merits of both distributed feedback (DFB) and distributed Bragg reflector (DBR) lasers was also performed during the program. The results from this study indicate that a second-order Bragg grating embedded in the confinement layer located directly above the active layer in a DFB type structure would provide the most stable longitudinal mode operation.

## HIGHLIGHTS

- Development of a quantum well (QW) ICSP diode laser.
- Laser threshold current reduced by 80%.
- Laser degradation rates <2 mW/Khr at 60 mW.
- Theoretically modeled DFB and DBR single-frequency lasers.
- Demonstrated DFB type structure will provide most stable single-frequency laser.

# Section I

# INTRODUCTION

Laser diode devices, to be qualified for space communication or other space applications, are required to have high reliability because of the cost and the difficulty of performing repair or maintenance tasks in the space environment. High power operation is required for laser sources in space communication to reduce the overall size of both the transmitter and receiving systems . Prior to the beginning of this work, the CSP laser was the best known AlGaAs diode laser structure for high power in a single spatial mode in the 780-870 nm wavelength range. CSP lasers developed under previous contracts have exhibited single spatial mode emission at output powers to 160 mW, with phase front aberrations less than 1/40 of a wavelength rms and power conversion efficiency exceeding 35%. It was therefore an excellent candidate for high power space communication.

The purpose of this program was to improve the reliability of high power 870 nm AlGaAs CSP lasers. The goal was to obtain 60 mW peak power with less than 2mW reduction in the output power per 1000 h at 25°C, with modulation at 100 MHz and 50% duty cycle. The far-field pattern, single spectral mode characteristics and polarization ratio should not degrade during 6000 h of aging under the above conditions.

In order to achieve the prescribed degradation rate at this high output power level, the CSP design must be optimized or improved, and the lasers must be mounted and tested under conditions that represent the working environment in space. Design improvement was to be obtained by modeling and computer simulation, by improving current confinement, and by improving our techniques for facet coating. Good current confinement would be achieved by the DCC-CSP

design (double current confinement-CSP), obtained by growing a p-blocking layer on the n-substrate before etching the channel for material growth. The mounting would be improved by mounting the laser in "M type" packages (TO-46 packages), instead of the so-called "L-mounts" that are often used for testing laser devices. In addition, wire bonding would be used to replace our customary indium solder to bond leads to the device. Finally, burn-in procedures are to be developed and lifetesting is to be performed to ensure that the delivered devices would indeed have the required performance characteristics.

Aside from the work on CSP lasers, a design study was to be made to enable the selection of distributed feedback (DFB) or distributed Bragg reflector (DBR) for a stable laser source. Fabry-Perot lasers, which rely on the combination of internal gain and facet reflection feedback to determine lasing threshold, have poor wavelength stability because of the close spacing of the longitudinal modes. Changes in optical length cause the lasing wavelength to shift or hop easily. Such changes can be induced by factors such as injection current (affects refractive index), temperature, and facet reflection (from external components). DFB and DBR lasers, which contain a grating in the optical path, have strong modal selectivity and, therefore, restrict feedback only to modes that fall within the Bragg region. The latter is strictly determined by material parameters (not external factors) and the grating period. Therefore, these types of lasers are excellent candidates as long term stable sources for operation in space. There are certain performance and fabrication differences between the two types, and one of the tasks in this program is to evaluate these two types of sources and make recommendations on a preferred choice.

In the course of this program, two major developments emerged that led us to shift attention away from CSP and toward a new design that we call ICSP (inverse CSP). First, we learned that in addition to their high drive current

requirements, (60-80 mA threshold current) the performance of CSP lasers strongly depends not only upon the width of both the contact stripe and the substrate channel in the substrate, but also on their relative alignment, which is difficult to achieve within the tolerances prescribed by modeling (less than 0.25μm). Operation at high power reveals modal instability and unacceptable degradation rate with time. The second development was the rapid evolution of MOCVD (metallo-organic chemical vapor deposition) as a reliable growth process that enables the deposition of uniform layers of III-V compounds even in the very thin configuration required for quantum-well (QW) devices. Quantum well lasers are known to provide low operating current by virtue of the effect of the film thickness on the density of states. The laser cavity can also be made longer in order to increase the net gain and achieve high power. Typical QW lasers have threshold current of 12-15 mA, about 5 times lower than their CSP counterparts.

CSP lasers require the growth of a uniform layer over a channel etched in the substrate. Such growth is readily feasible with the liquid phase epitaxial (LPE) growth technique, but not with MOCVD. The ICSP laser uses a smooth substrate and, therefore, is well suited for MOCVD growth. Its guiding properties, which are similar to that of the CSP, are obtained by etching away part of the p-clad material outside the lasing area, and regrowing GaAs to planarize the structure and provide the desired lateral loss responsible for the CSP type of operation.

In view of the above findings and developments, the program was redirected toward the fabrication and testing of ICSP lasers grown by MOCVD. We successfully made and tested these devices. It is this type of device that constituted the deliverables under this contract.

We report here first, on the work performed on the design, fabrication, mounting, and testing of CSP lasers and on the results on their lifetest. Then, we proceed with our development and lifetest of ICSP lasers, the type that qualified for delivery. A section is included on the assessment of DFB and DBR.

# Section II

# HIGH POWER CSP LASERS

## 1. BASELINE CSP

### a. Design and Fabrication of CSP Lasers.

The design of CSP lasers was optimized by computer modeling. The optimized design for an emission wavelength of 870 nm is shown schematically in Fig. II-1.

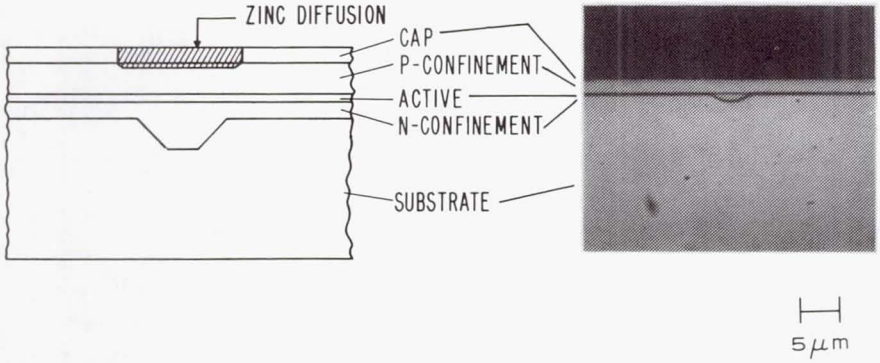


Figure II-1. Schematic diagram and cross-section micrograph of the CSP laser optimized for 870 nm emission wavelength.

The structure is fabricated in a single-growth-step using liquid phase epitaxy (LPE). V-shaped channels are chemically etched in the (100) oriented GaAs substrate along the [011] direction using an oxide-defined contact mask before LPE growth. Prior to placement of the substrate in the horizontal sliding graphite growth boat, the entire surface of the wafer is subject to a light chemical etch. This procedure ensures that both the surfaces in the channel region and on the substrate are chemically prepared in the same manner for LPE growth.

LPE growth is performed over the V-channeled substrate and four layers are grown: (1) $Al_xGa_{1-x}As$ cladding layer (x = 0.27, 0.3 μm, $N_d = 1 \times 10^{18}$ $cm^{-3}$); (2)

GaAs active layer (0.07 μm, $N_d = 1 \times 10^{17}$ $cm^{-3}$); (3) $Al_xGa_{1-x}As$ cladding layer (x = 0.27, 1.5 μm, $N_a = 5 \times 10^{17}$ $cm^{-3}$); (4) GaAs capping layer (0.7 μm, $N_d = 5 \times 10^{17}$ $cm^{-3}$). The growth is performed at 800°C using a cooling rate of 1°C/min. The fabrication of high-power CSP lasers having the proper lateral index profile for fundamental mode operation requires the active layer to be planar over the V-channel while the thickness of the n-cladding layer outside the channel region is maintained between 0.2 and 0.5 μm. A non-planar active layer alters the lateral index profile of the CSP structure, which degrades the superior performance characteristics of the laser. To ensure planar active-layer growth over the channel region, it is necessary to maximize the total amount of supercooling associated with the gallium melt used for the growth of the n-cladding layer. This is accomplished in our automated growth system by using the single-phase growth method [1] for the n-cladding layer and the two-phase method [2] for the growth of the other layers in the CSP structure. The single-phase growth method permits us to accurately control the degree of supercooling present in the gallium melt prior to the introduction of the growth wafer. In addition to the quick filling of the V-channel to planarize the layer, careful control of the amount of supercooling also permits a high degree of control on layer thickness not only across the wafer but from one LPE growth run to another. The single-phase growth technique may also be used for the growth of the other layers in the structure, but is not necessary since the n-cladding layer grown directly on the non-planar substrate planarizes the surface for the subsequent layers. The use of the single-phase growth technique for all the layers in the structure would unnecessarily complicate the growth process.

Another factor effecting the planarity of the active layer in the CSP structure is the crystal orientation of growth substrate. The effects of surface morphology due to large amounts (> 0.5°) of substrate misorientation with respect

to the (100) surface has been previously noted in the literature.[3] We have found that substrate misorientations as small as 0.1° may result in terracing of the n-cladding and active layers in the CSP structure during the LPE growth process. The terrace must be eliminated before the growth of the active layer, otherwise the change in the active layer thickness due to the terrace alters the lateral index profile of CSP structure. By optimizing the LPE growth conditions and minimizing the misorientation of the growth substrate with respect to the (100) plane, planar active layer growth can be obtained on a routine basis. Micrographs of a CSP with and without terracing as shown in Fig. II-2.

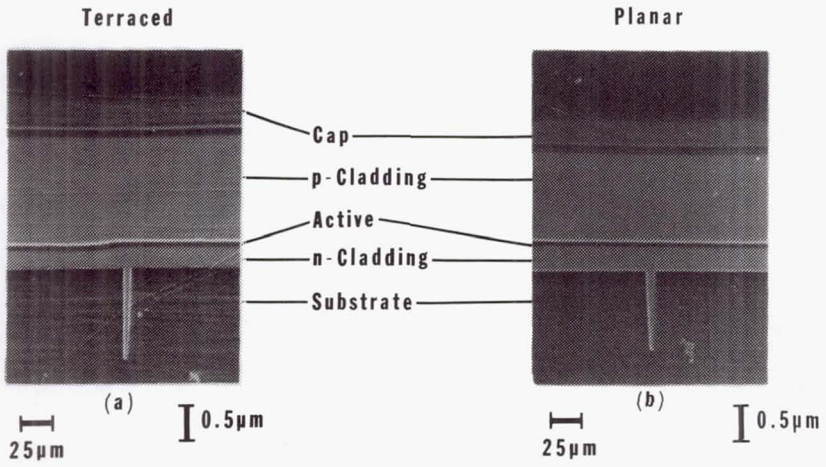


Figure II-2. Micrographs of two CSP growths angle-lapped at 1° angle showing (a) terraced and (b) non-terraced active layer.

The flow of current in the CSP structure is confined to the channel region via a deep zinc diffusion. Zinc is diffused through the n-type cap layer into the p-type cladding layer using an oxide-defined contact mask, thereby forming a reverse bias p-n junction to confine the current flow. The leading edge of the zinc front is positioned approximately 0.5 μm above the active layer.

### b. Characteristics of High Power CSP Lasers

CSP lasers have been fabricated that have produced lasing operation to 205-mW cw, single-fundamental-spatial and spectral-mode operation up to 100 mW (50% duty-cycle), with single-spatial mode operation continuing up to 160-mW cw. Beyond 160 mW increasing line broadening was observed in the parallel far-field pattern due to gain saturation effects and the existence of higher order modes.

Figure II-3 shows the power output vs drive current (P-I) curves for a CSP laser. The device is 200 μm long, with a ($\lambda/4$) $Al_2O_3$ passivation coating on the (front) emitting facet and a six-layer dielectric-stack reflector on the rear facet. In Fig. II-3a, we show the performance of the CSP laser as the heatsink temperature is varied from 0°C to 80°C. Note that 80-mW-cw output power was obtained at a heatsink temperature of 80°C. The device operated in a stable single-spatial mode over the entire temperature range. The differential quantum efficiency decreased from 62% to 45% as the heatsink temperature was raised from 0°C to 80°C. The $T_o$ value in cw operation over this temperature range is approximately 100°K. At 62% differential quantum efficiency, the slope efficiency is 0.89 mW/mA.

Figure II-3b shows the results of operating a device to its catastrophic optical damage (COD) level. Damage occurred at 205 mW cw at a drive current of 335 mA. The applied voltage at 205 mW is 1.76 V. The emitting facet displayed melting of the crystalline material, normally associated with facet damage. This exceptionally high COD level was attained without the use of a window type structure.[4] The differential quantum efficiency was 55% at the COD level. Also displayed in this figure is the total power conversion efficiency from the emitting facet of the device from the lasing threshold value to the maximum cw output power level. The peak power conversion efficiency was >35%. The high power conversion efficiency, which permits single-mode operation at high output powers

and temperatures, is associated with the optimization of the current flow and mode control in the CSP structure. Attention to the control of these parameters using improved growth and processing procedures should ultimately lead to high reliability at high power.

The spectral behavior of the optimized CSP structure at high power level is shown in Fig. II-4. Predominantly single-longitudinal-mode operation was achieved to (a) 100 mW cw and (b) 100 mW 50% duty-cycle of output power. At higher output powers, the intensity ratio of main mode to the satellite modes decreases with increasing drive, thereby degrading the single-longitudinal-mode qualities of the device. Spectral changes with increasing output levels reflect increases in junction temperature due to joule heating effects. At 100 mW, the CSP laser operates at approximately three times the threshold current.

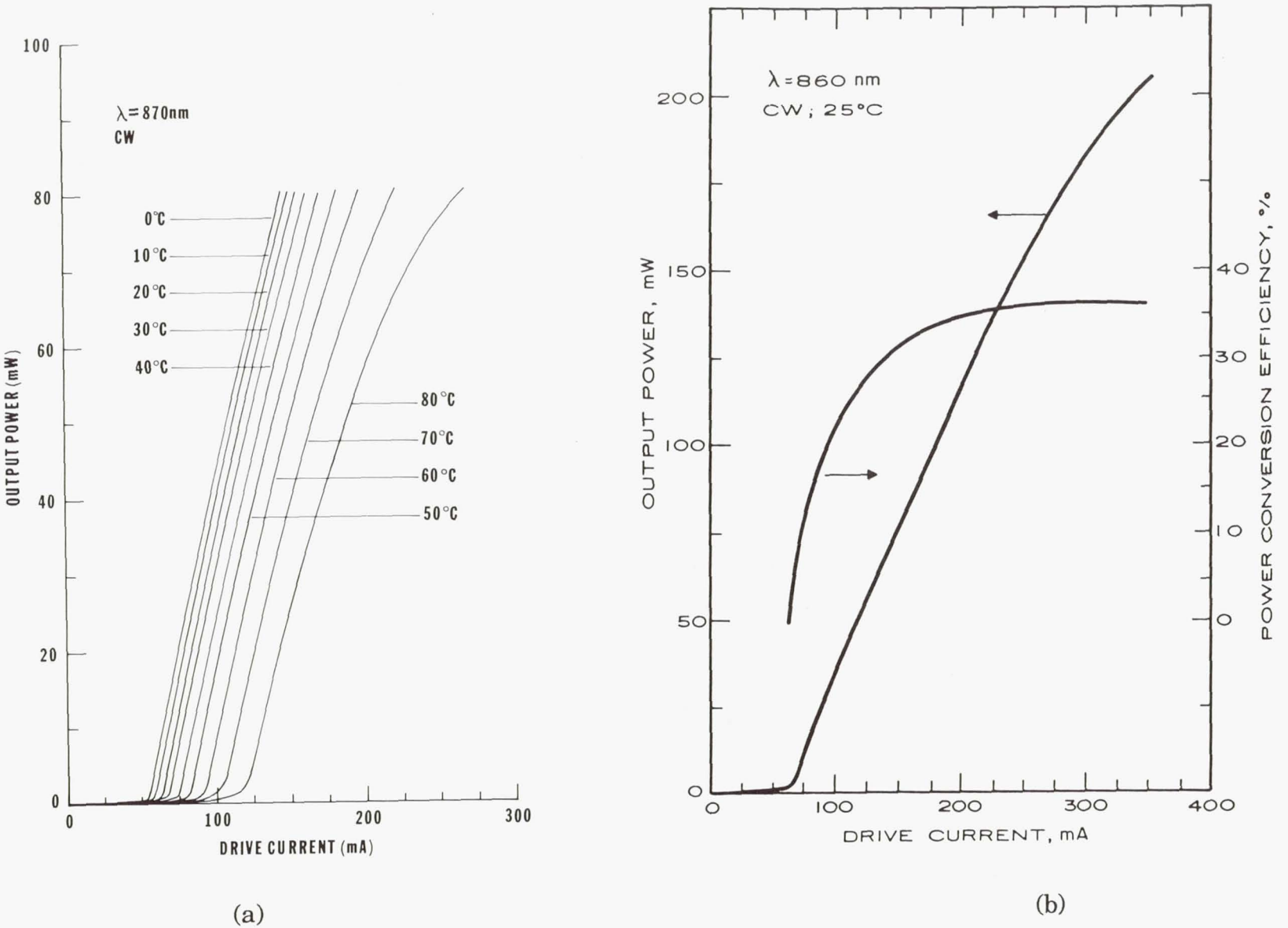


Figure II-3. Power output vs operating current (P-I) curve for a CSP laser at (a) various heatsink temperatures and, (b) when operated to its catastrophic optical damage (COD) level.

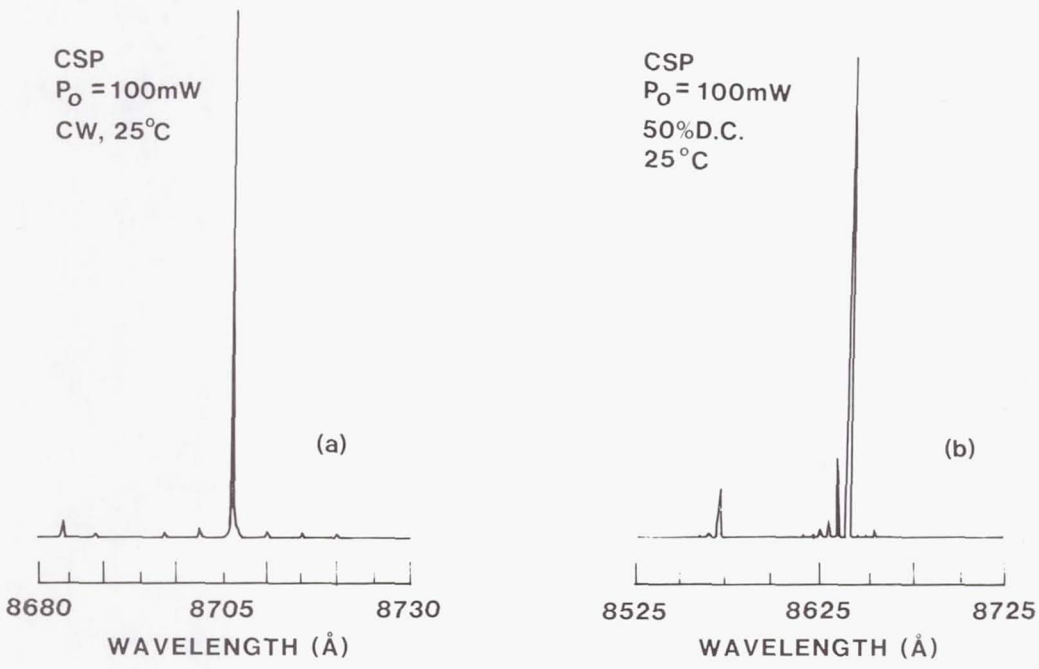


Figure II-4. Longitudinal-mode spectrum for a CSP laser operating at 100 mW in the (a) cw and (b) 50% duty-cycle modes.

The lateral and perpendicular far-field patterns of an optimized CSP laser from 100 mW to 190 mW of cw output power are shown in Fig. II-5. Below 100 mW, the beam full width at half-power (FWHP) of the lateral far-field patterns remained unchanged with drive current. At output powers of 100 mW and above the beam FWHP broadens from 11° to 15° with increasing drive current due to heating and gain saturation in the CSP structure. The perpendicular far-field pattern did not change with increasing drive current, the beam FWHP remains unchanged at 25°. At output powers exceeding 190 mW, higher order mode operation begins to dominate until the COD level is reached.

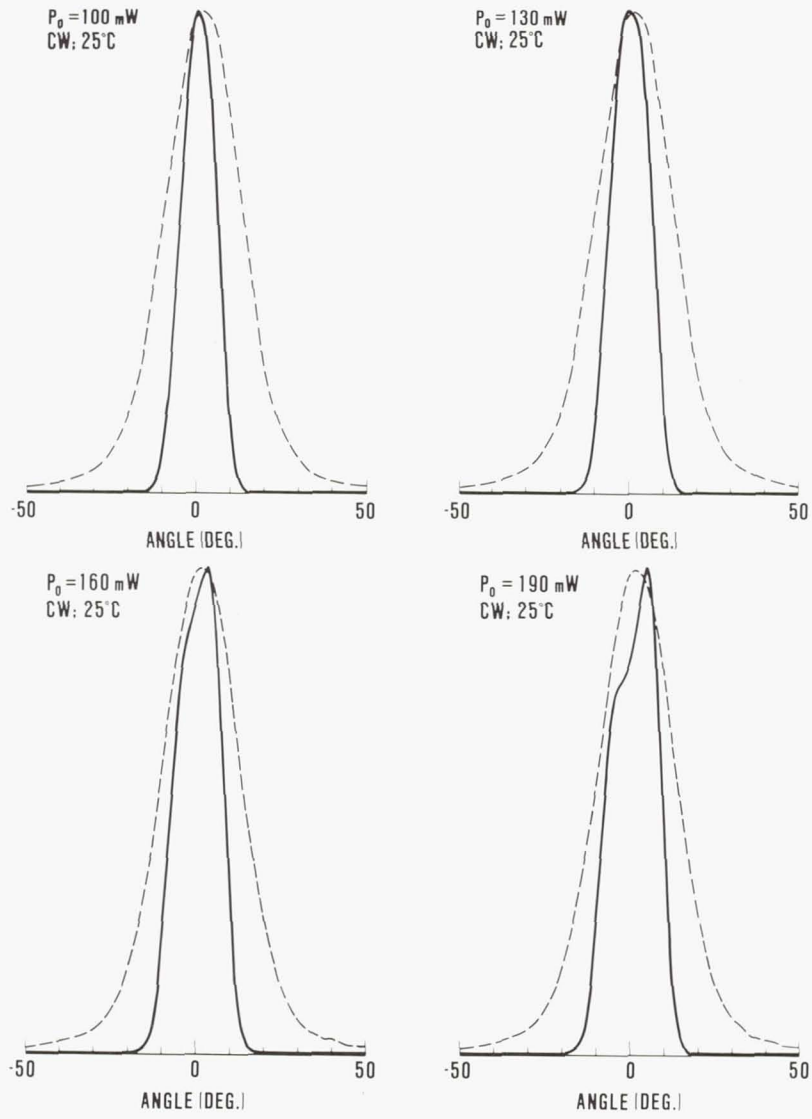


Figure II-5. Lateral and perpendicular far-field radiation patterns for a CSP laser operating from 100- to 190-mW cw.

## 2. BASELINE DCC-CSP

### a. Design and Fabrication of DCC-CSP Lasers

Despite the significant improvements made to the CSP structure that have resulted in devices exhibiting lower threshold currents and record efficiencies, further refinements were still required to reduce the drive current level for reliability at high power. According to our model, the incorporation of one or

more current blocking layers would effectively focus the current to the lasing area and improve differential quantum efficiency. One approach to incorporating a blocking layer into the CSP structure is by growing a layer(s) prior to channel etching and LPE growth by using MOCVD growth techniques having a doping of polarity opposite to that of the GaAs substrate. A schematic representation of the CSP laser with an internal current blocking layer, is shown in Fig. II-6. We call this structure the double current confined-channel substrate planar laser or DCC-CSP laser. In order for the blocking layer to be effective, its thickness should be greater than the minority carrier diffusion length. Otherwise, current will flow through it. On the other hand, as shown in Fig. II-6, since the V-channel must be etched through it, it cannot be made too thick, otherwise the channel would be too wide and would allow the propagation of high-order waveguide modes.

We found that the barrier layer thickness should be below 1.2 μm in order to prevent multimode operation. At a doping concentration comparable to the substrate, this thickness is more than the hole diffusion length, but it is less than required to block electron flow because of the electrons higher mobility. To reduce the electron diffusion length in this p-type blocking layer to below 1.2 μm, one can take advantage of the fact that the electron diffusion length is a function of doping concentration and material composition. Increased doping concentration of one order of magnitude is difficult to achieve with LPE growth, but is readily possible by using MOCVD growth. Thus, we use MOCVD to grow the blocking layer. The use of AlGaAs as a blocking layer would also reduce the electron diffusion length because of its composition. However, due to the formation of surface oxides, it is difficult to grow new layers on the AlGaAs. Thus, the procedure we chose for the blocking layer is to first grow $Al_{0.1}$ $Ga_{0.9}$ As for the main blocking function, then follow it by a thin layer of GaAs as the base for the subsequent regrowth.

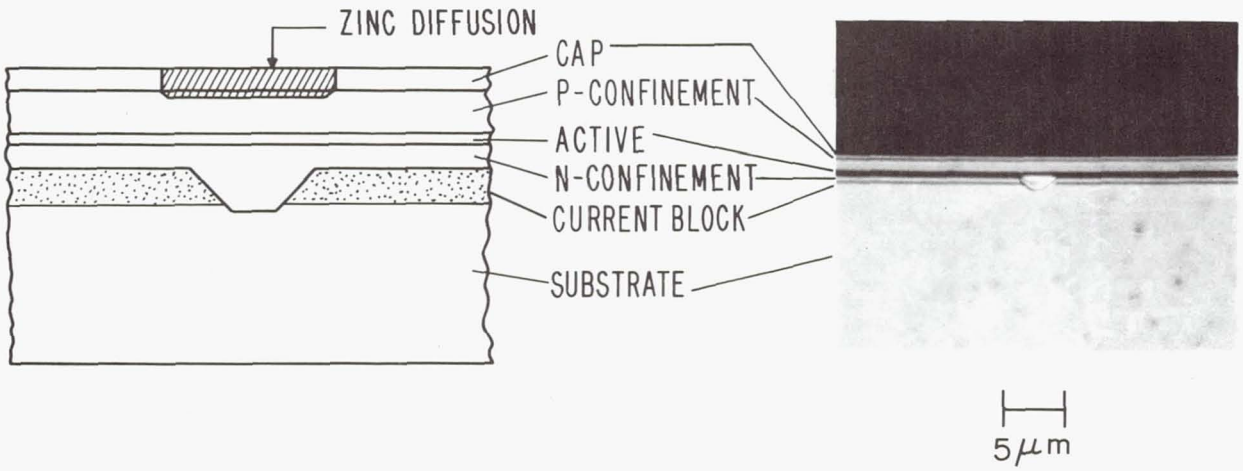


Figure II-6. Schematic diagram and cross-sectional micrograph of the DCC-CSP laser structure.

### b. Characteristics of DCC-CSP Lasers

Several LPE growth runs incorporating the new current blocking layer have been characterized. In Fig. II-7a and II-7b, the output power vs drive current and corresponding far-field radiation patterns are displayed. The output power was measured both in the cw and 50% duty-cycle mode at a heatsink temperature of 25°C. The laser was operated up to 35 mW and 70 mW, respectively. The differential quantum efficiency remained unchanged at 70% for both modes of operation.

The perpendicular and lateral far-field radiation patterns for the DCC-CSP laser are displayed in Fig. II-7b. They were measured in both the cw and 50% duty-cycle mode of operation. The lateral far-field pattern was measured at 30 mW cw and 70 mW 50% duty-cycle. The beam full width at half power (FWHP) remained unchanged at 7°, indicating that no movement of the lasing spot occurred with output power or operating conditions. The perpendicular far-field radiation pattern was measured at 70 mW 50% duty-cycle and the FWHP was 22°. These measurements were conducted at a heatsink temperature of 25°C.

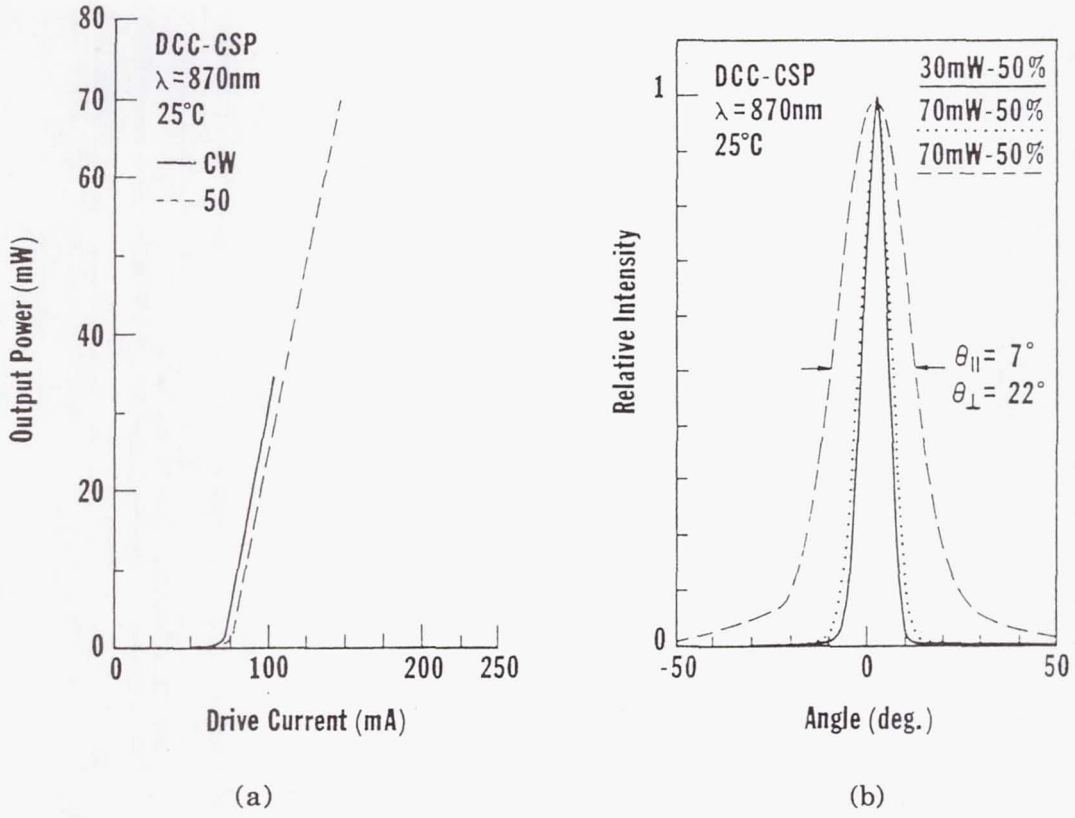


Figure II-7. (a) Power output vs operating current (P-I) curve and (b) lateral and perpendicular far-field radiation patterns for a DCC-CSP laser.

The spectral characteristics of the DCC-CSP laser are shown in Fig. II-8. The spectrum was measured at a heatsink temperature of 25°C and under both cw and 50% duty-cycle operation. Single-longitudinal-mode operation was displayed under both operating conditions at the same peak emission wavelength of 866.2 nm. The extremely high efficiency of the device significantly reduces the heating effects in the laser, thus, permitting operation at the same peak wavelength at different power and operating conditions. The small amount of spectral broadening observed in the 50% duty-cycle mode is associated with chirping of the longitudinal mode during the pulse.

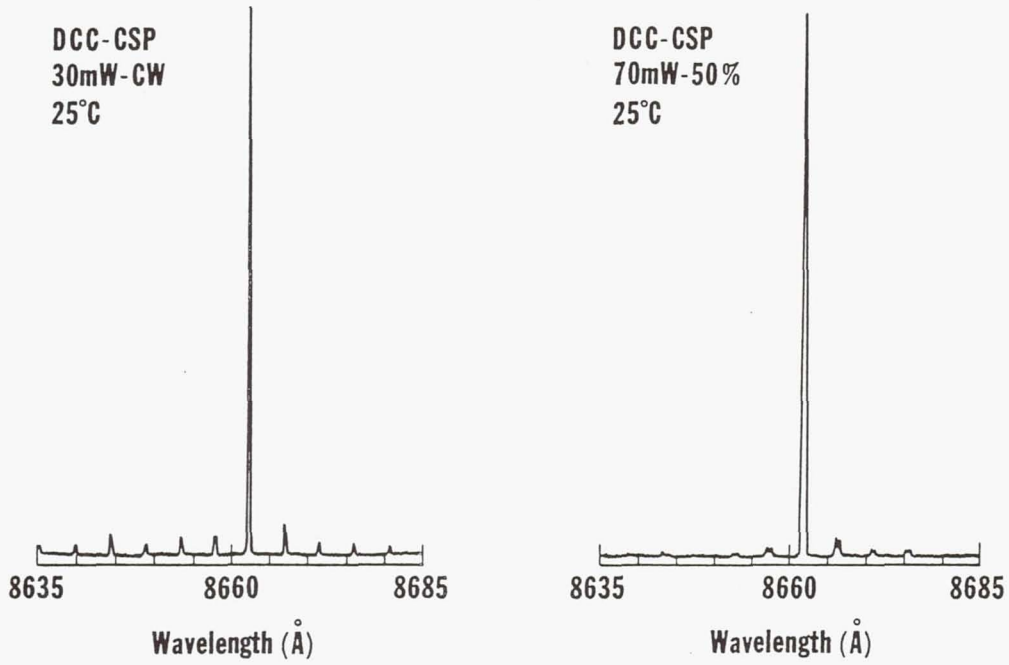


(a) (b)

Figure II-8. Longitudinal mode spectrum for a DCC-CSP laser operating (a) cw and (b) 50% duty-cycle at an output power level of 35 mW and 70 mW, respectively.

# Section III

# TESTING CSP LASERS

## 1. EQUIPMENT

### a. Modification of Lifetest Racks

The program required lifetesting to be done under 50% modulation at 100 MHz with devices mounted on commercial "M-mounts." Our test racks were originally designed for operation at 10 MHz, and for devices bonded on our customary "L-type" mounts. Therefore, one of the first tasks on this program was to modify the existing lifetest racks to operate under the new conditions.

New circuits were designed for the drive electronics to operate at 100 MHz. The circuits deliver a constant bias current just below lasing threshold, on which is added the high frequency modulation current by AC coupling. In this work, the circuits were designed to provide a modulation current of 100 mA, which is considered adequate, since the current level required for the prescribed output of 60 mW is typically about 50-75 mA above threshold. It is very important to avoid electrical transients caused by power surges which may occur during storms or other causes of power fluctuation. Electrical transients that apply more than about 8 volts to the laser can break down the laser junction and short circuit or degrade the device. In order to avoid this type of damage during lifetest, the system's power supply was designed with latching relays intended to shut it off in the event of a power failure and to prevent restarting once power is restored. Restart is done manually by resetting the relays.

A new fixture was built into the diode holders in the lifetest racks to accept the M-type mounts in place of the L-mounts. These M-type mounts are the same as the standard Philips TO-46 packages that are sold commercially. Their design includes a window that can be used as a hermetically sealed cap.

A third modification in the test equipment was the replacement of the detectors used to measure the light output of the lasers by a fiber optic bundle that can feed either an integrating sphere or a spectrum analyzer. The lifetest equipment consists of 3 racks, each containing 6 test positions, for a total test capability of 18 diodes simultaneously. Normally, each test position is equipped with a photodetector mounted about 2 in. in front of the laser. Due to the beam divergence of the lasers, the detector captures only a fraction of the total light output, but this fraction is proportional to the total output power. We found that this method of measurement is accurate to only about $\pm 10\%$. In order to capture more light, the detector must be brought close to the laser facet, but the present design of the laser holder does not allow this flexibility. However, the testing specifications require the discrimination of 2 mW out of 60 mW over a period of 1000 h, equivalent to a change of 3%. Thus, a measurement accuracy of better than 3% is required in order to obtain an accurate assessment of the degradation rate. In addition to power, wavelength stability was to be determined as well.

This problem was resolved by using the arrangement shown in Fig. III-1. A fixture with an attached fiber bundle is made to bring the fiber tip to about 1 mm from the diode facet, thus capturing the maximum amount of light. In order to measure output power, the other end of the fiber is positioned within an integrating sphere, which gives an accurate measurement of the output power to within less than 3%. This tip can also be placed inside a spectrometer to measure the wavelength. Thus, the arrangement provides *in situ* measurements of the two critical parameters connected to degradation. A photograph of two six-position lifetest stations is shown in Fig. III-2.

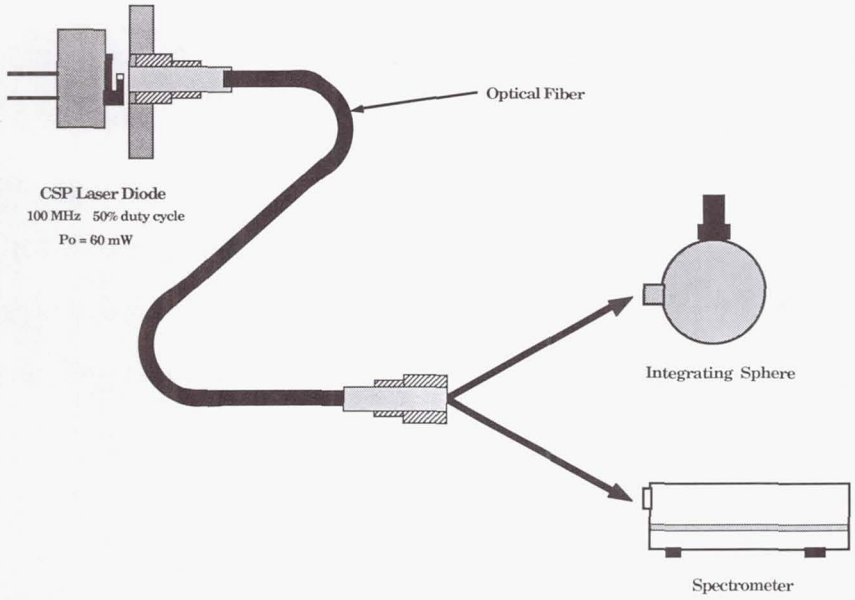


Figure III-1 Arrangement using fiber, integrating sphere and spectrometer to accurately measure laser diode power and wavelength during lifetest.

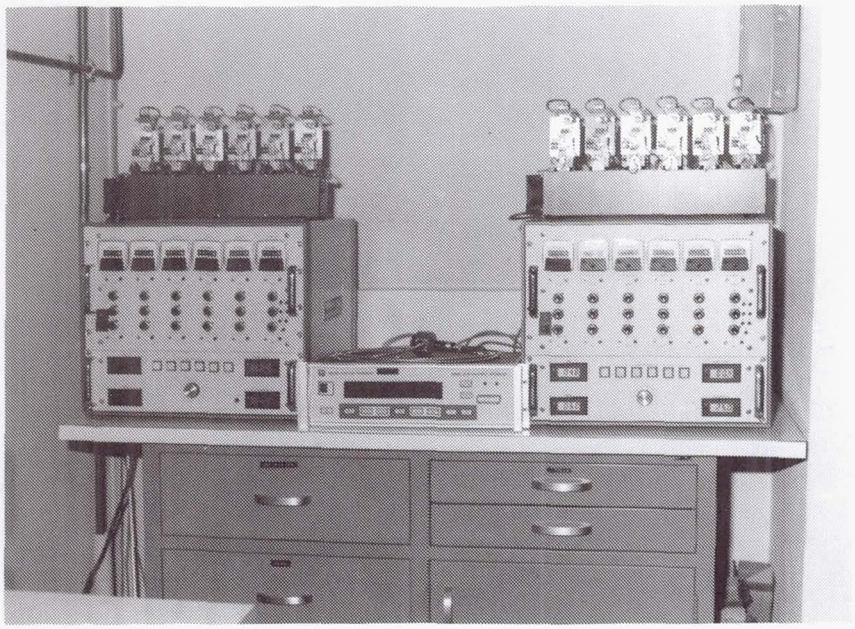

Figure III-2. Photograph of lifetest set-up showing two six-position stations.

A separate station was built for burn-in of the lasers prior to lifetesting and weed out infant mortality. In the initial plan, we intended to use the lifetest system for burn-in as well as lifetesting. However, as the number of diodes available for testing increased, it became necessary to create a separate station for burn-in. Thus, a separate 12-position station was built for that function. DC current was used for that purpose, as it was intended only for screening purpose. A photograph of the burn-in station is shown in Fig. III-3.

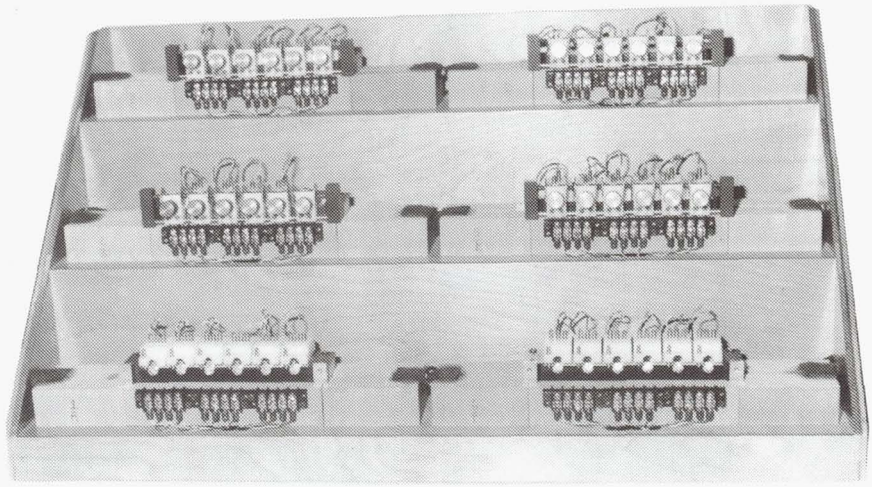

Figure III-3. Photograph of 12-position burn-in station.

**b. Laser Mounts**

The M mounts for this program were purchased from Sumitomo Electric Inc. They consist of three parts: a base containing a wedge shaped platform to serve as a heatsink on which the laser can be mounted, a feed-thru section for the leads that is welded to the base, and a window section that can be hermetically sealed to the rest of the unit. An engineering drawing of this mount is shown in Fig. III-4. Since these mounts contain much less thermal mass than the L-mounts, an evaluation was performed to determine their heat transfer capacity.

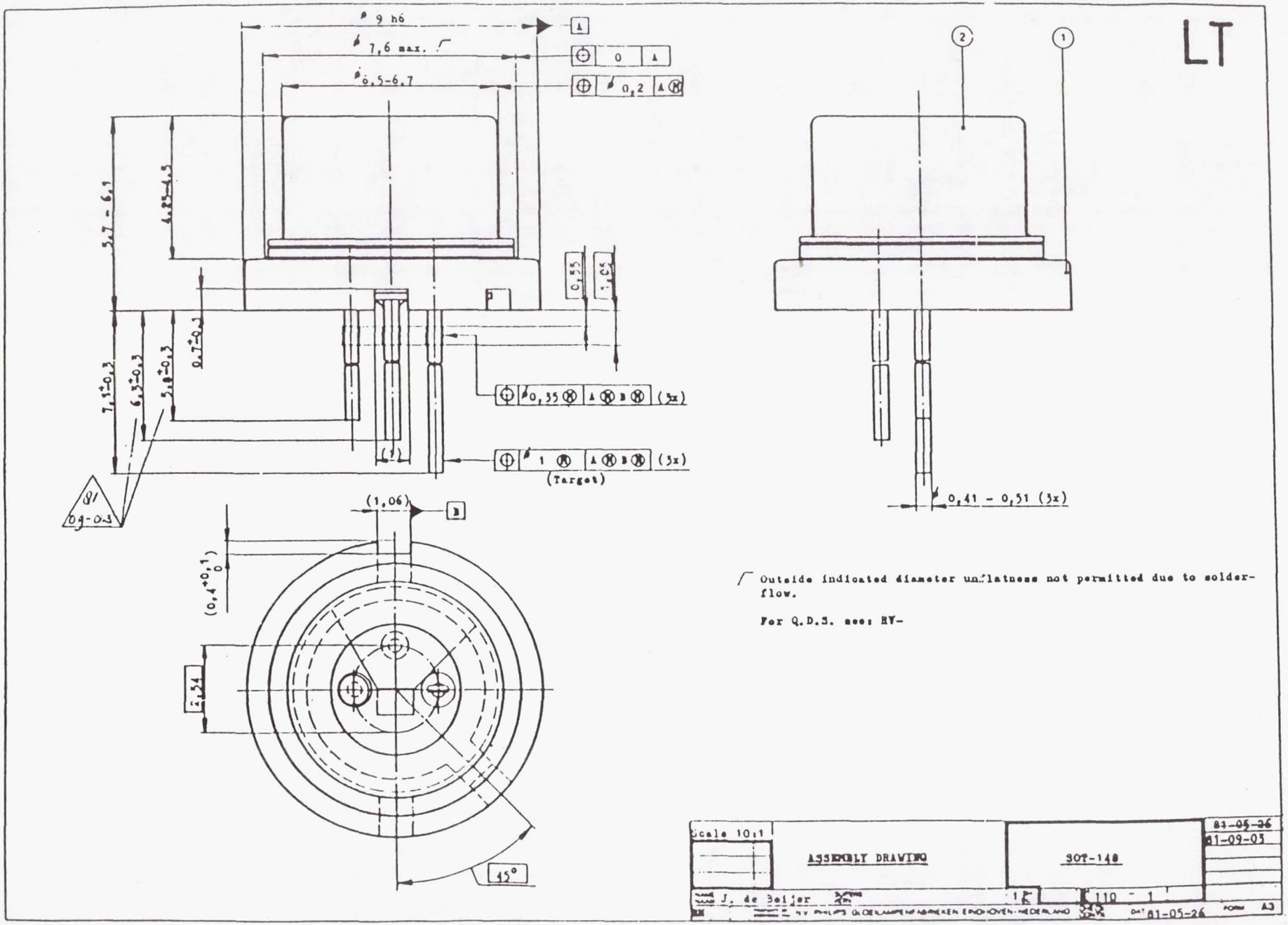


Figure III-4. Schematic diagram of package used for mounting the CSP laser.

Test samples of both L and M mounts were modified to permit temperature measurements at various points on the mounts as a function of input electrical power. The results of these measurements were used to estimate the laser junction temperature increase. The L packages showed a temperature increase of 2-3°C, and the M packages showed temperature increase roughly twice as large (4-6°C). Although slightly inferior to the L mount, this performance is considered adequate, since this temperature rise is significantly smaller than the values (30-40°C) that can cause thermal degradation.

We did find two problems with the M mounts. One is the gold plating, the other is the weld joint between the base and the lead feed-thru. These packages were plated by the manufacturer with Ni followed by a thick layer of Au. We soldered laser diodes on them using our SnAu plated Cu preforms. Voids were observed in the solder bonds, apparently caused by the thick gold layer drawing away the Sn from underneath the chip. These voids have high thermal resistance and cause large increase in the junction temperature. The total thickness of the gold on the package must be controlled in order to obtain an ideal Au-Sn eutectic solder bond. In order to obtain better control of the gold thickness, we decided to order the packages only with Ni plating from the manufacturer and to perform the Au plating in our own facilities. A sample lot of 50 Ni-plated packages were received and Au-plated. Fifteen CSP lasers from LPE growth TJ-277 were machine-mounted on them using a Au/Sn eutectic solder. Figure III-5a and 5b are photographs of one of the mounted devices. All the mounted lasers displayed uniform bond thickness and excellent wetting under the entire chip. The devices were examined on our automated characterization equipment at both 30 mW cw and 60 mW 50% duty cycle. Basaed upon the characterization results obtained from the lasers, the Au plating process was judged adequate for mounting lifetest

lifetest devices. Additional quantities of the new Ni-plated M mounts were received and Au-plated in our facilities.

(a)

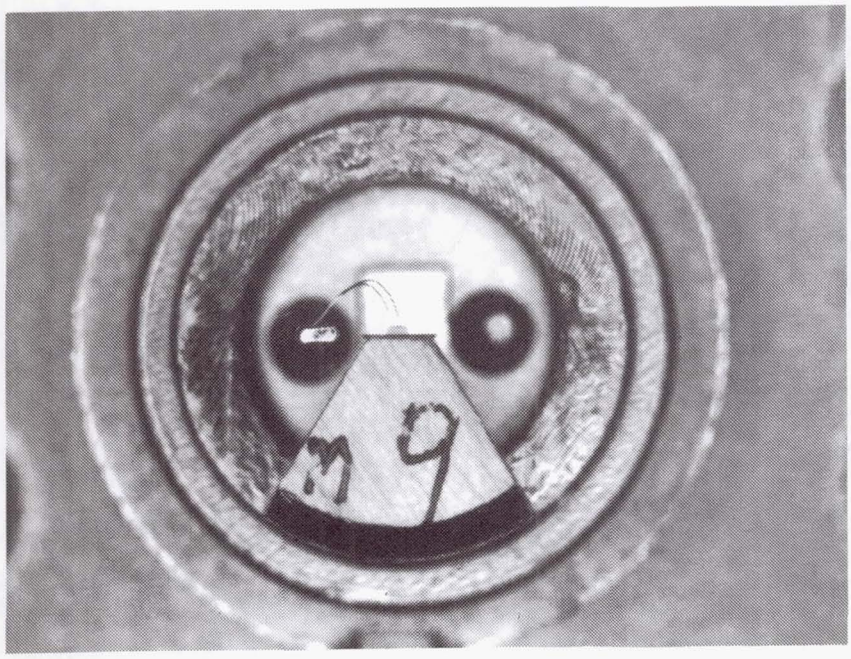


(b)

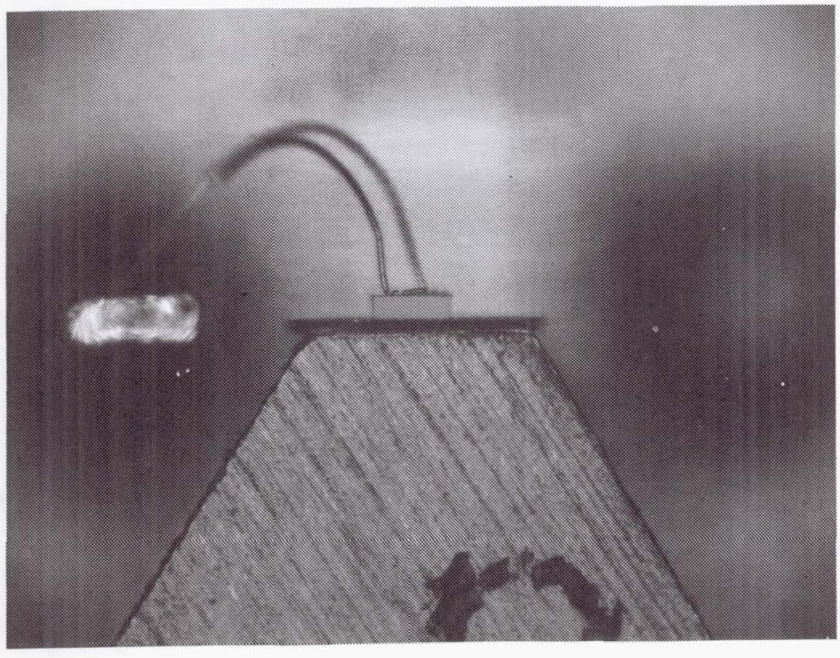

Figure III-5. Photographs of diode bonded to M mount a) complete package, and b) close-up of laser showing laser and preform.

The other problem was a separation that occurred in some packages at the weld joint between the base and the lead feed-thru, which caused the n-side wirebond to pull away from the laser chip. This problem was reported to the manufacturer who promised to correct it and did, but with a six month time delay. During the six month delay, we re-worked the packages in house and sent them to an outside vendor for welding. The re-worked packages were leak tested and found to perform adequately. We were ready for lifetesting CSP lasers.

## 2. CSP LIFETESTING

### a. Growth and Characterization

Four high-power channeled substrate planar (CSP) wafers were grown using our automated liquid phase epitaxial (LPE) growth system. All four wafers exhibited a planar active layer above the channeled region in the CSP structure. Planarity in the active layer is essential to avoid displaying kinks in the optical power versus operating current curve (P-I) or low optical output power from the devices. The planarity of each wafer is monitored using an angle-lapping technique. A photograph from one of the grown wafers is shown in Fig. III-6. The thickness and composition of the layers in the CSP structure are listed in the figure. These wafers were processed and devices made from them were characterized for suitability as lifetesting candidates.

A lot of fifty-five CSP laser chips (TJ-277) were probed under pulse operating conditions to test the threshold current value and slope efficiency. A total of twenty-eight chips satisfied the specified threshold current ($I_{th}$< 75 mA) and efficiency ($\eta$>50%) requirements. These chips were mounted on "M-style" packages and were characterized for threshold current, series resistance, forward voltage, slope efficiency, far-field radiation patterns, and spectrum. All devices were characterized under both cw and 50% duty cycle operating conditions

and were operated to 60 mW peak output power. The average threshold current and emission wavelength for the twenty eight devices were 70 mA and 870 nm, respectively. The perpendicular and lateral far-field radiations patterns measured at the beam full width half power (FWHP) location were 7° and 27°, respectively.

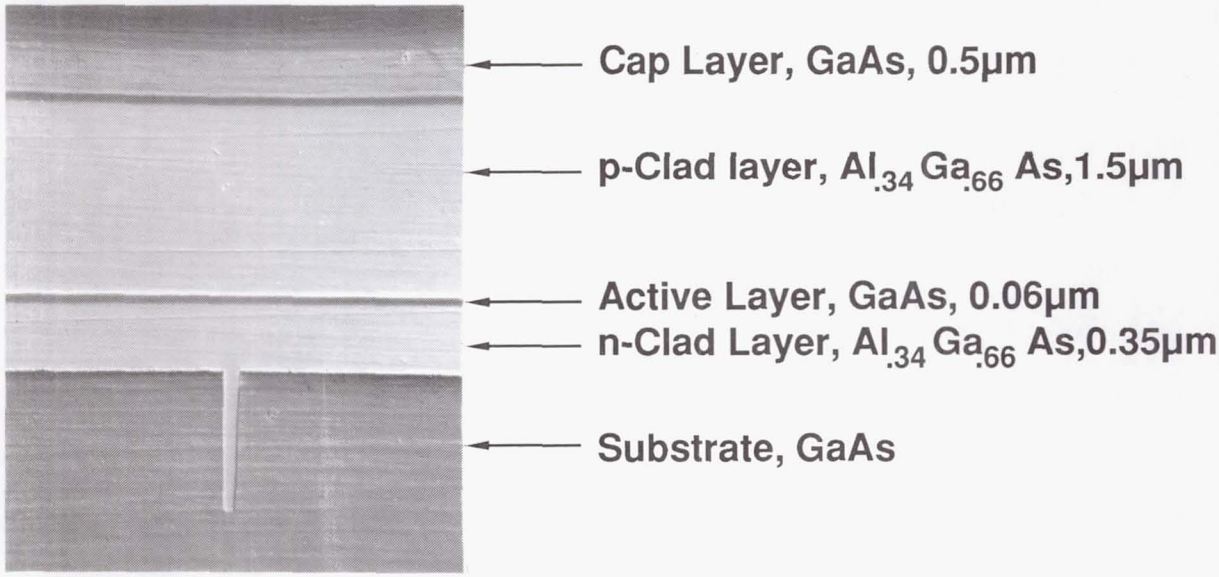


Figure III-6. Angle-lap showing planarity of active layer over CSP channel.

Ten devices were chosen as candidates for lifetesting from the twenty-eight devices after our screening procedure. The objective of this screening procedure is to eliminate devices which would degrade prematurely. The screening procedure involves examination for smooth and linear P-I curve to rated power, stable I-V characteristics, and a stable longitudinal mode spectrum. An example of such a screened device is shown in Figs. III-7 to III-9. In Fig. III-7, the P-I curve, taken under both cw and 50% duty cycle conditions, is shown along with the I-V characteristics for the device. The cw threshold current for the device is 76 mA with a series resistance of 2.7 Ω. The perpendicular and lateral far-field radiation patterns are shown in Fig. III-8. The beam full width at the half power (FWHP) point were 25° and 6.5°, respectively. The beam remained stable with

increased output power and exhibited no movement. The predominantly single longitudinal mode spectrum is displayed in Fig. III-9. A stable single mode was obtained at a wavelength of 868 nm with no indication of any other Fabry-Perot modes present. The devices are also given a visual inspection under a optical microscope to identify any physical damage which may cause premature failure. Once the device has passed these tests, it is ready for the 200 h burn-in procedure.

The burn-in procedure is similar to the lifetest procedures except that it is carried out for a relatively short period of time. Probe testing, which is done under low-duty cycle pulsed condition, only indicates features such as threshold current, operating wavelength, linearity of P-I characteristics and capability to reach rated power. Burn-in is performed under normal or accelerated working conditions under which devices containing defects would not survive a long time. Such devices degrade rapidly early in their life, during the first 100 to 200 h. Only those that survive this "infant mortality" test need to be lifetested. Thus, burn-in is another level of screening in the process of device selection.

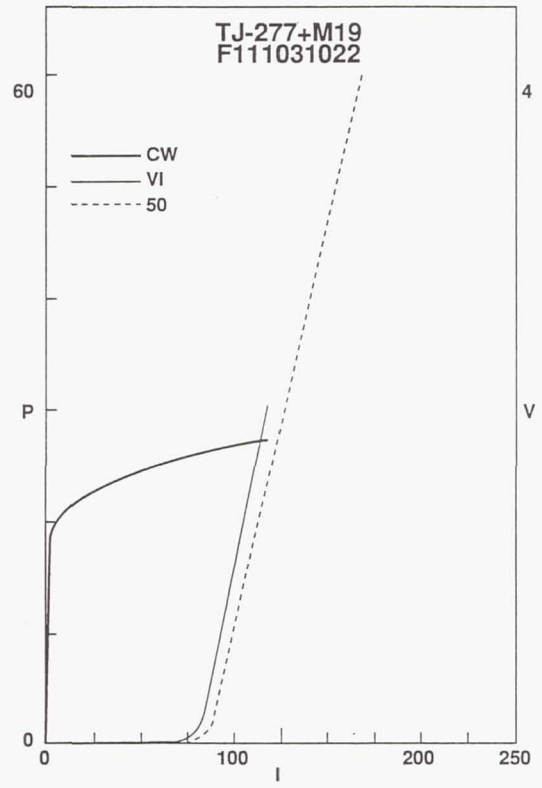


Figure III-7. P-I characteristics of probe-tested laser selected for burn in.

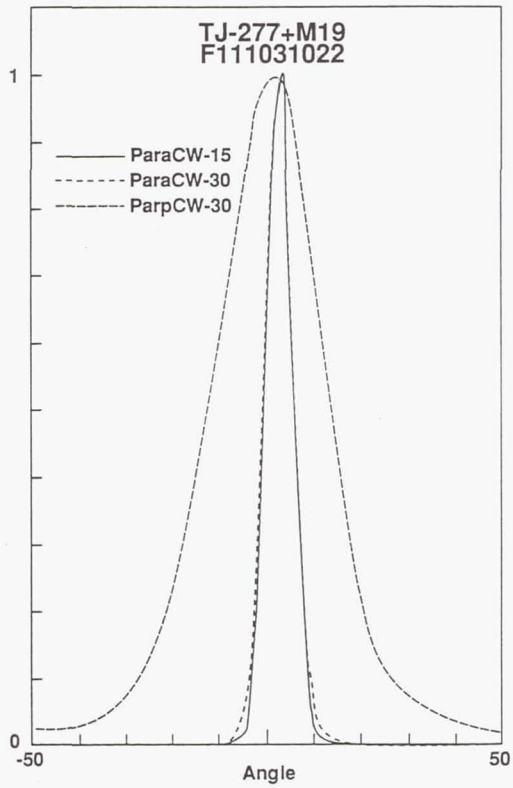


Figure III-8. Perpendicular and lateral far-field pattern of probe-tested laser selected for burn-in.

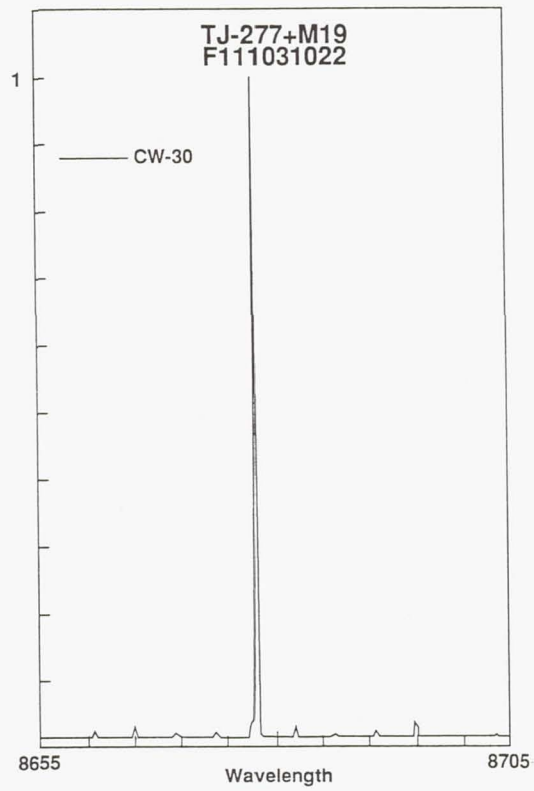


Figure III-9. Spectrum of probe-tested laser selected for burn-in.

Lifetesting is done by setting the devices in the lifetest racks, driving and operating them under rated conditions, and periodically measuring and comparing performance to prescribed specifications. The specifications were:

- Maintain 60 mW peak power at 25°C under 50% duty modulation at 100 MHz, with degradation rate less than 2 mW per 100 h.

- In addition, the far-field pattern, single spectral mode characteristics and polarization ratio should not degrade during 6000 h of aging under the above conditions

### b. Lifetest Performance

Several batches of diodes from the four wafers that exhibited planar layers were fabricated and tested. In one group of experiments, ten devices from LPE growth run TJ-277 which satisfied the probe tests, were placed on the ten racks for burn-in. Five devices failed in burn-in, showing rapid degradation or no light emission after a short time. The remaining five were left on the lifetest racks, but they continued to degrade at different rates, as shown in Fig. III-10. The best device of the lot, device No. M6, had a degradation rate of about 8mW/Kh, a value that is four times the desired performance.

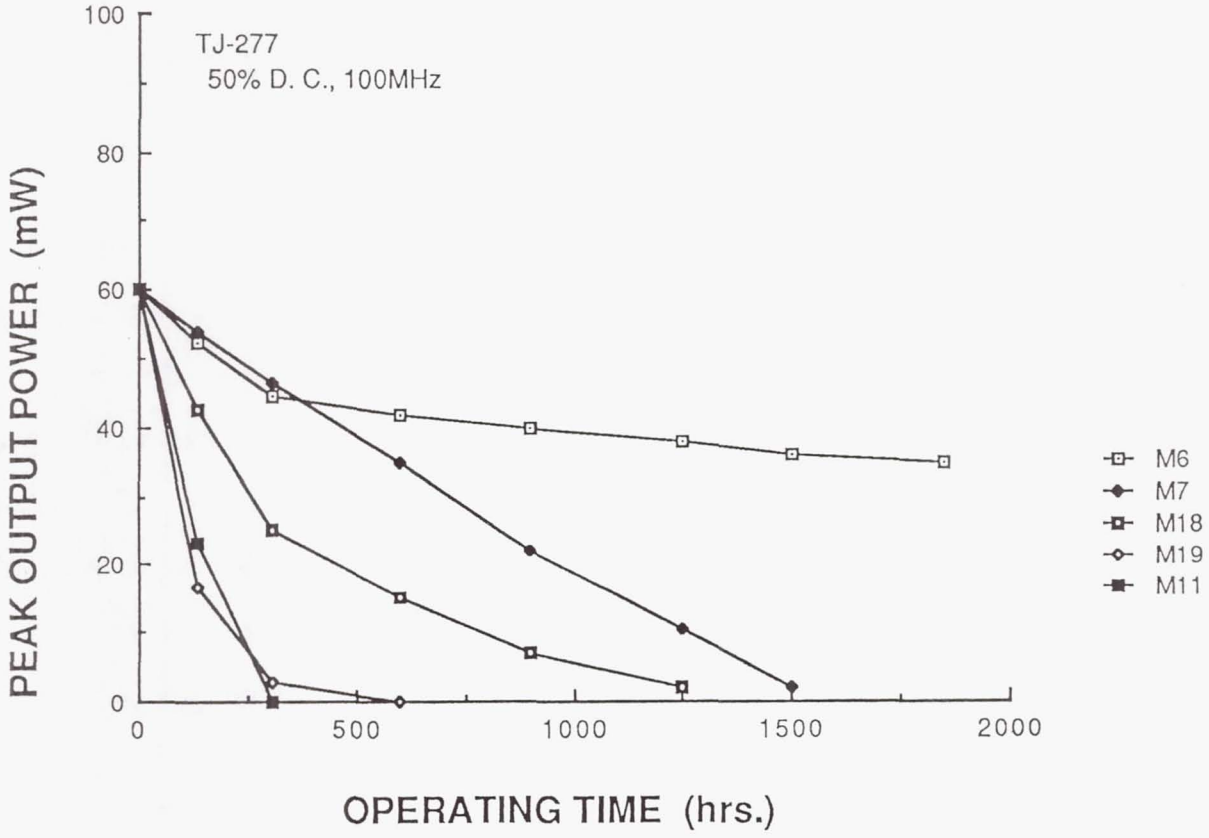


Figure III-10. Degradation of lasers from run TJ-277 during lifetest at constant current and 100 MHz modulation. Initial condition 60 mW peak.

A second set of devices from a different LPE growth run (TJ-273) were placed on lifetest. A lot of sixty chips were probed under pulse operating conditions to test the threshold current value, I-V characteristics, and slope efficiency. A total of twenty-seven chips satisfied these specifications and were mounted on the "M-style" packages for further testing. The mounted lasers were characterized for threshold current, series resistance, forward voltage, slope efficiency, far-field radiation patterns, and spectrum. All devices were characterized under both cw and 50% duty-cycle operating conditions and were operated to 60 mW of peak output power. The average threshold current and emission wavelength for the twenty-seven devices were 73.5 mA and 872 nm, respectively. The typical perpendicular and lateral far-field radiations patterns measured at the beam full width half power (FWHP) location were 8° and 27°, respectively.

Seven devices were chosen as possible lifetest candidates from the twenty-seven devices after our screening procedure. As before, the devices were placed on burn-in operating at a peak output power level of 60 mW under 50% duty-cycle conditions. Two of them were discarded because of infant mortality. The remaining five lasers were lifetested. As found with the lot from TJ-277, the devices from TJ-273 also showed a constant degradation rate with operating lifetime. One of them became unstable at approximately 500 hours of life and was removed from the test. Another one degraded rapidly and would no longer emit light at approximately 775 hours. The remaining three devices degraded in a manner that was similar to that observed for LPE growth run TJ-277.

These observed degradation rates at 60 mW are far in excess of the program goal of 2 mW/kh. They also exceed the rate we had previously obtained for lasers operating at a peak output power level of 50 mW. We would not expect such a large increase in degradation rate with only a 20% increase in peak output power.

The consistency of the degradation rates among lasers fabricated from the same wafer and among lasers from different wafers leads us to conclude either that accelerated degradation does occur in CSP lasers above a certain power level, or that additional mechanisms are at play in these new batches. At any rate, it was certain that continued lifetesting of more devices from TJ-273 and TJ-277 would exhibit the same poor degradation rates as with the first lots tested. Hence, the focus of our effort was channeled towards the identification of the degradation mechanism responsible for the poor performance of the device, and towards the development of improved devices.

### c. CSP Assessment in Light of New Technologies

Excessive heating is considered to be the cause of the poor performance of our CSP devices under sustained high power operation. With this view in mind, we examined the three recognized causes of heating of laser diode devices; thermal resistance, electrical resistance, and excessive internal losses.

We examined the change in the peak of the spontaneous emission wavelength with operating conditions and found it to indicate higher internal temperatures than expected. The normal thermal resistance for mounted CSP type lasers is generally between 20-40 °C/W. A junction temperature of ~100°C higher than the heatsink temperature would correspond to a thermal resistance value of about 200 °C/W. These high values would cause the lasers to operate at a temperature 4-5 times higher than normal, hence severely shortening device life. We also examined both the quality of the laser chip bond and the laser chip itself to determine the source of the thermal impedance. The bond quality was found to be quite consistent and of good quality for all the devices examined. Thermal resistance was probably not the problem.

Heating can also be caused by high series resistance. Low doping concentration and poor metallization can be the cause of high electrical resistance. However, we did not observe any physical evidence of poor metallization or measure any excessively high electrical resistance. Thus, a re-examination of the CSP structure at high power was necessary.

We believe that the culprit is the excessive losses that occur in the CSP at high power, due to slight misalignment between the channel and the zinc diffusion stripe in the CSP structure. Computer analysis indicates that the optimum CSP design requires the zinc diffusion stripe to be narrower than the channel and to be well centered with respect to it. If the stripe overlaps the channel, there is high gain and high optical field at the wing where the overlap occurs. Optical absorption, hence heating, is very high at that location, due to the proximity of the GaAs substrate to the active layer in the regions outside the channel. This heating is reduced if the stripe is narrower than the channel, provided that their alignment is within less than a fraction of a micron to present any possibility of overlap. Such alignment is difficult to achieve because there is a difference of only about one micron between the two different widths, and because the CSP is not a self-aligned structure. Figure III-11 shows how the misalignment can cause heating in the CSP. The misalignment shifts the gain profile toward the wing of the channel where more light is generated and absorbed, causing saturation at low power levels.

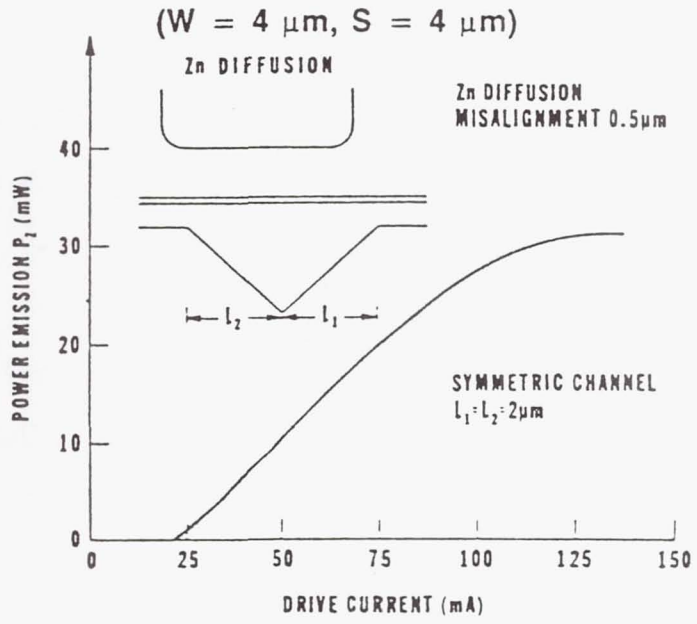


Figure III-11. Power saturation caused by heating due to misalignment of stripe and channel in the CSP laser.

The lifetesting of the liquid phase epitaxial (LPE) grown CSP laser devices was suspended at the request of the COTR at NASA Langley Research Center to re-direct the efforts of the program towards the development of a more reliable metal organic chemical vapor deposition (MOCVD) grown laser device. The original goal of this program was to provide 30-60 mW LPE-grown diode lasers demonstrating good reliability. During the course of the program, however, the state-of-the-art technology for high-power AlGaAs diode lasers advanced quite rapidly due to the ongoing development of MOCVD growth and re-growth processes. This improvement in MOCVD methods has led to the reported development of low threshold current and high quantum efficiency index-guided quantum well (QW) laser structures. The lower threshold current and higher power conversion efficiency make conventional double-heterostructure (DH) diode

lasers obsolete. Hence, the completion of this program using LPE-grown CSP lasers would not provide NASA with a true state-of-the-art laser device for its space communication systems. The remaining effort on the program, therefore, was directed towards the development of a QW laser structure grown by MOCVD techniques.

# Section IV

# HIGH POWER ICSP MOCVD-GROWN QW LASERS

## 1. ICSP LASER

### a. Design

We have seen that the CSP structure is not self-aligned, and that its performance is critically affected by the alignment between the V-channel and the zinc diffusion stripe. In addition, the nature of LPE growth limits its abiility to produce highly uniformily thick layers. Growth non-uniformity and poor stripe alignment have caused the yield of high power CSP lasers to be low. A QW structure is desired that is self-aligned and that can be grown by MOCVD that provides uniform growth. A laser structure that meets these requirements is the inverse CSP (ICSP). A schematic diagram of the QW ICSP laser structure grown at Sarnoff is illustrated in Fig. IV-1

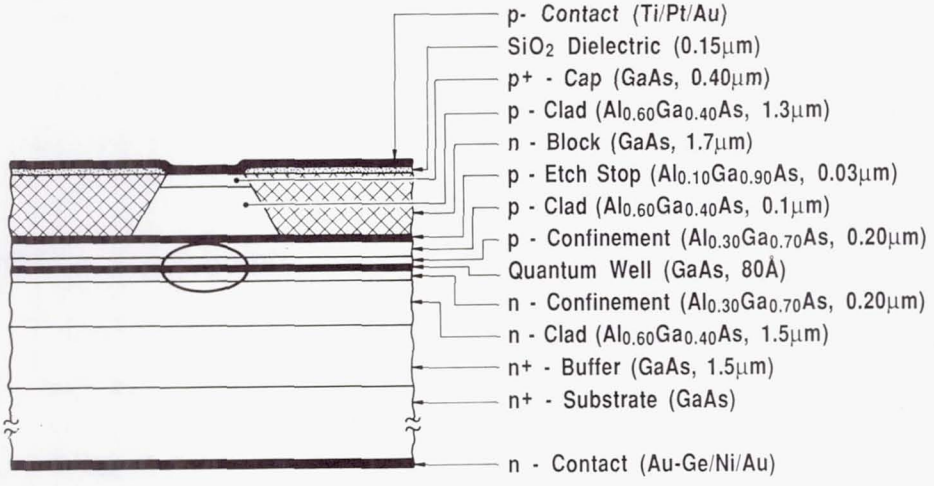


Figure IV-1. Schematic diagram of the QW ICSP structure.

Basically, it is a laser structure in which the p-clad outside of the stripe is partially replaced by a layer that absorbs light at the laser emission wavelength, in order to obtain the loss-guiding characteristics of CSP that result in single lateral mode at high power. In AlGaAs lasers, this absorbing layer can be GaAs. It is created by regrowth after an etching step that removes the p-clad everywhere except along a ridge or mesa that defines the laser waveguide. The regrown GaAs region is illustrated by the crosshatched portions of the figure.

**b. Fabrication**

The first step in the ICSP fabrication process is the MOCVD growth of the nine layers of the laser structure. The thickness and composition for each of the layers is described in Fig. IV-1. The thickness of the GaAs quantum well is chosen to provide a lasing wavelength of ~ 830 nm.

The first stage in the formation of the mesa region is the deposition of a $SiO_2$ dielectric film (~1000 Å thickness) on the wafer surface to prevent material from depositing on top of the mesa during the second MOCVD growth step. The film is densified at 800°C to stabilized the film for MOCVD growth. Stripes having a 7 μm width and aligned along the (011) direction are formed on top of the $SiO_2$ film by photolithography. The spacing between stripes is 300 μm. The photoresist mask serves two functions: 1) as a mask for opening stripes in the $SiO_2$ film, and 2) as a mask for the etching process used to form the mesa of the ICSP structure. This etching is done in two steps to ensure accurate control of the etch depth with minimum undercutting of the mask. The undercutting is a critical parameter since it directly impacts the width of the mesa region and therefore the lateral mode control in the structure. The first etchant which totally removes the GaAs cap layer and partially removes the AlGaAs clad layer is 1:8:8 ($H_2SO_4$:$H_2O_2$:$H_2O$). This is an isotropic etchant that leaves behind a mirrored surface. The etch rate

at 20°C for this etchant is about 4 μm/min. The second etchant is 1:4 ($HF:H_2O$) which selectively etches $Al_xGa_{1-x}As$ for x values larger than 0.3. The etch rate for the 1:4 etchant at 20°C is about 1 μm/min. During the $H_2O$ rinse between the two etching steps the wafer is kept submerged to prevent oxidation of the p-clad layer. If oxidation is present on the wafer surface prior to the second etching step, non-uniform etching or non-etching of the p-clad layer will be observed. After the second etch step, approximately 0.2 μm of p-clad layer remains to provide the lateral index step for fundamental mode operation. The photoresist mask is removed after the etching procedure for the next fabrication step, the MOCVD growth of the current-blocking layer. In this growth process, a 1.7 μm thick GaAs layer is grown on the wafer. Deposition is prevented on the mesa structure by retaining the $SiO_2$ mask used to form it. The surface kinetics of the MOCVD growth process are such that no deposition occurs on that $SiO_2$ surface. Prior to layer deposition, the wafer surface is annealed for twenty minutes at 700°C under an arsenic-rich environment to remove native oxide formation from the AlGaAs surfaces. This treatment improves the growth nucleation on these surfaces,and provides excellent surface morphology and layer uniformity across the entire wafer.

The conductivity of the regrown layer is chosen such that it is reversed biased when the applied current to the laser is in the forward bias direction. This effectively confines the current flow in the laser through the mesa region only, and eliminates the need for a deep zinc diffusion process as in the conventional CSP laser structure. In addition, the correct conductivity permits the lateral guiding and the current injection to be self-aligned, a problem that plagued the conventional CSP laser structure. The elimination of this zinc diffusion process should also impact reliability. In addition to the required alignment to the buried channel, the zinc diffusion process also requires accurate depth control with

respect to the active layer. If the zinc front is greater than 1 μm from the active layer, excess current spreading leads to high threshold current and unstable far-field radiation patterns. On the other hand, if it is too close to the active layer (<0.3 μm), the zinc may diffuse slowly toward the active layer during operation of the laser leading to short circuits developing in the device and reduced lifetime. Thus the elimination of the deep zinc diffusion process is important to both the performance and reliability of the laser.

After the second MOCVD growth step, the $SiO_2$ mask on the mesa regions is removed using plasma etching, and a 1000 Å thick $SiO_2$ film is CVD deposited on the wafer surface. A photolitographic step in conjunction with plasma processing is used to define a 3 μm wide contact stripe on top of the mesa region, and a p-contact film of Ti/Pt/Au is deposited on this surface by electron beam evaporation techniques. The next step in the processing of the ICSP wafer is its mechanical/chemical thinning on the substrate side to 100 μm total thickness for subsequent cleaving processes, followed by the electron-beam evaporation of the n-contact film consisting of Au-Ge/Ni/Au. This film is then alloyed for 10 minutes at 450°C to promote ohmic contact. Finally, the wafer is cleaved into 500 μm long bars and the facets are coated. The emitting facet coating is a $Al_2O_3$ film with a reflectivity of 32%, and the rear facet is coated with a reflector consisting of six alternating $\lambda/4$ layers of $Al_2O_3$ and Si for a reflectivity of about 90%. After facet coating, the bars are cleaved once again to form the individual laser chips. The chips are probe tested for output power versus operating current (P-I), operating current versus forward voltage (I-V) and slope efficiency. Only those chips demonstrating superior operating characteristics are selected for mounting on the TO-46 package.

Figure IV-2a-c shows actual photographs of cross-sections of the ICSP structure at various stages of fabrication. Figure IV-2a represents the structure after etching the p-clad, leaving the mesa structure covered with the $SiO_2$ mask. Figure IV-2b shows a planar structure obtained after regrowth. The $SiO_2$ has been left on the mesa to prevent epitaxial growth over the mesa. Figure IV-2c shows the completed device, with a Ti-Pt-Au contact layer over the whole wafer.

A top view of the processed wafer after regrowth is shown in Fig. IV-3a, and the region near a stripe in the $SiO_2$ mask is shown in Fig. IV-3b illustrating the uniformity of the regrown layer and the absence of growth on the $SiO_2$ mask.

Figure IV-4 is a block diagram of the process flow from start of growth to completion of ICSP lasers. The process is straight-forward except that some care must be exercised to remove contamination of the etched areas prior to regrowth.

An interesting feature of ICSP structures is that some performance tests can be made immediately after the creation of the ridges to ascertain growth quality. Figure IV-5 illustrates a ridge laser made simply by metal coating a portion of the wafer. This step has been used to show that our QW ICSP structures have low threshold and linear characteristics to beyond 30mW cw, and to beyond 60 mW at 50% duty cycle, with high differential quantum efficiency at room temperature. Such characteristics are shown in Fig. IV-6 for a group of 10 lasers on the same chip (two of them were damaged in handling), demonstrating threshold of 12 to 15 mA, and only about 40 mA of drive current for cw output power of 30 mW. The far-field radiation pattern has a full width half power (FWHP) of 50° by 9°.

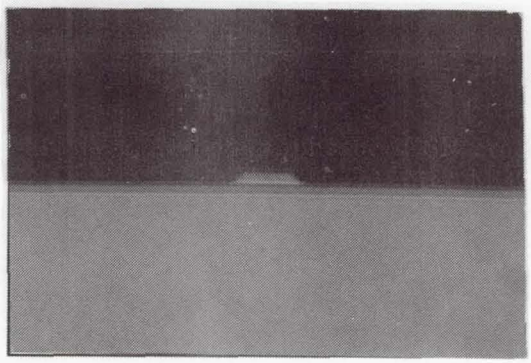

Base Structure Showing ICSP MESA

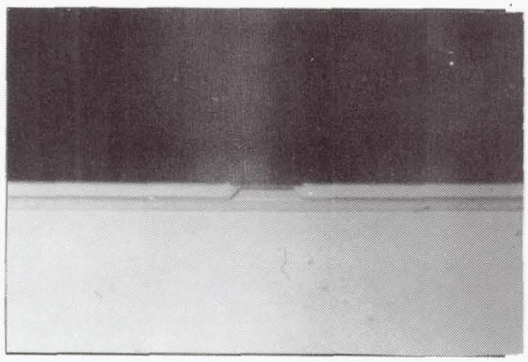

After MOCVD Regrowth With $SiO_2$ Mask

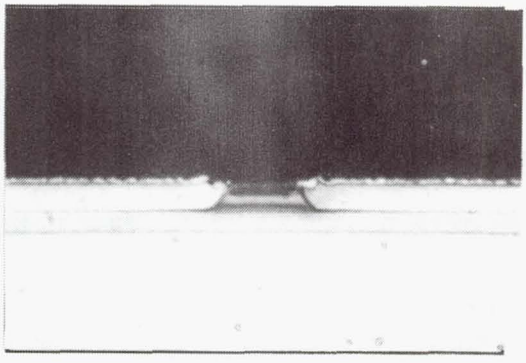

Fabricated Device

Figure IV-2. Photographs of ICSP cross-section at various processing stages. a) etched mesa, b) after MOCVD regrowth, c) fabricated device with p-metal electrode.

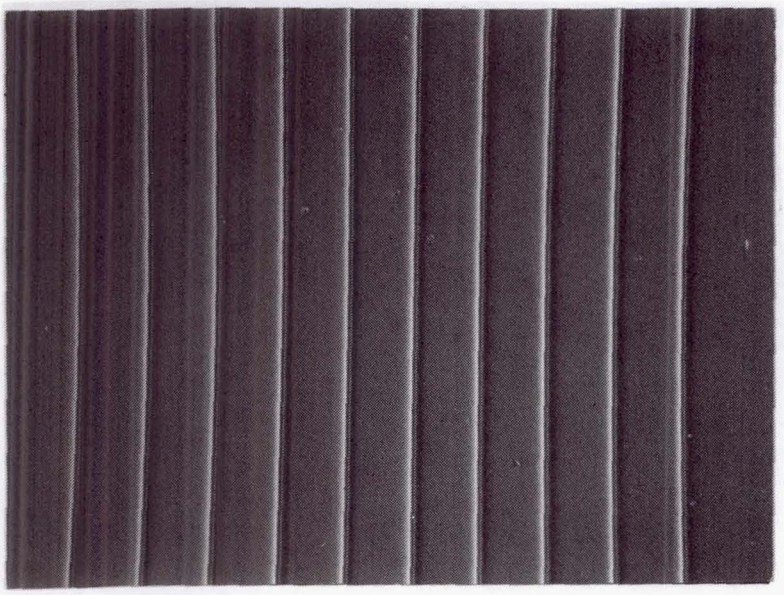

Wafer Surface
After MOCVD
Regrowth

(a)

300 μm

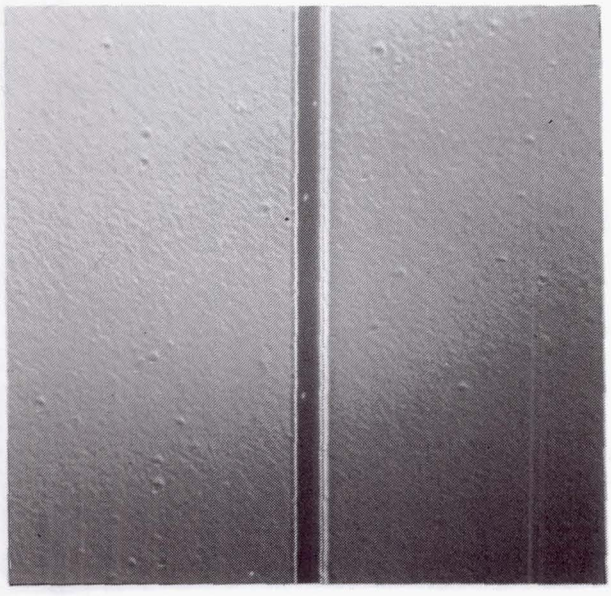

Single Element
With $SiO_2$ Mask

(b)

25 μm

Figure IV-3. Top view of processed wafer. a) after regrowth, b) stripe in $SiO_2$ mask showing no regrowth over $SiO_2$.

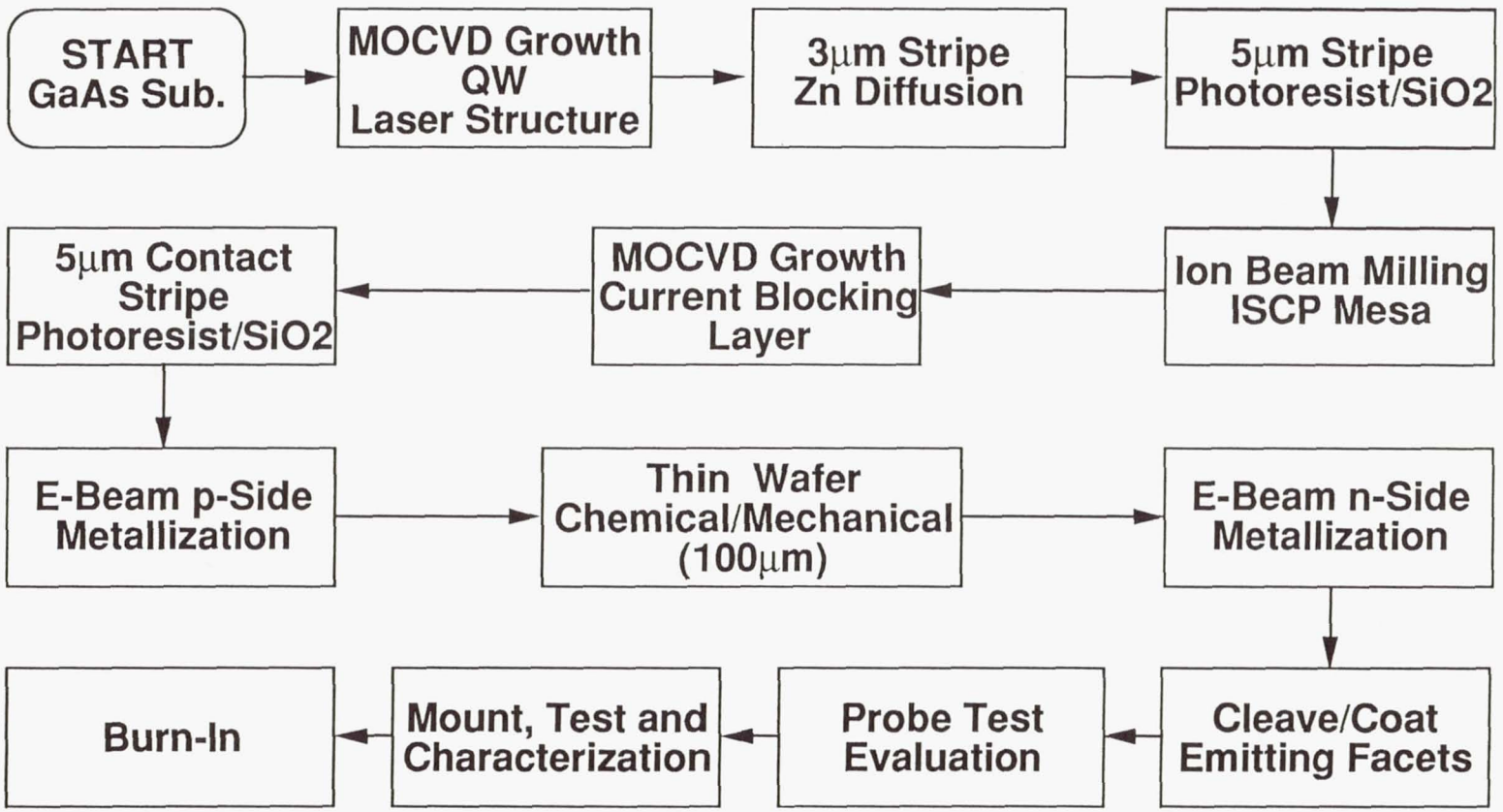


Figure IV-4. Process steps for ICSP arrays.

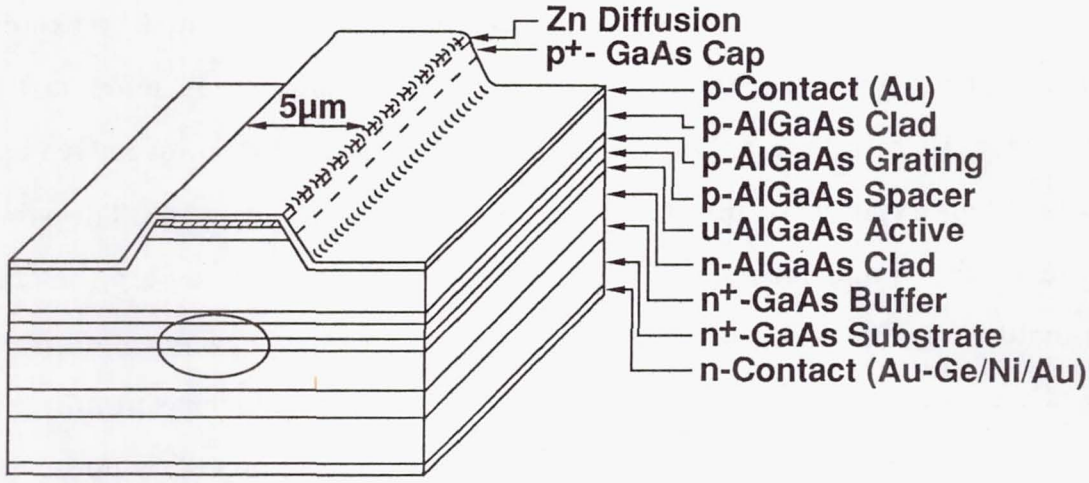


Figure IV-5. Ridge laser made from ICSP structure to evaluate wafer growth quality.

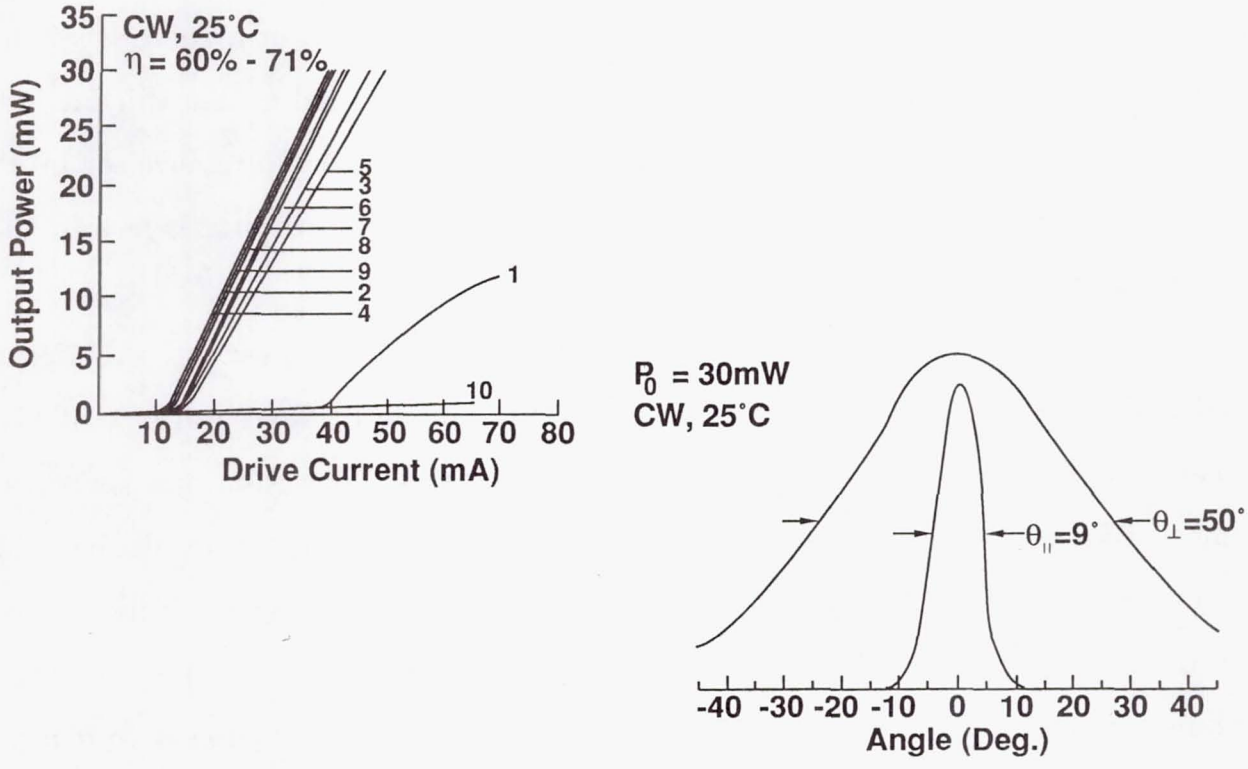


Figure IV-6. Characteristics of ridge laser array made from ICSP structure, showing low threshold and linearity at high power (Diodes No. 1 and No. 10 were damaged in handling).

### c. Regrowth Over AlGaAs

In the fabrication of lasers that require regrowth, care must be exercised in order to obtain good regrowth over established layers. It is more difficult to regrow over AlGaAs than to regrow over GaAs. The formation of native oxide on AlGaAs when exposed to air impedes epitaxial growth over it. Therefore, the oxide or surface impurity must be removed prior to regrowth, a step that must be done inside the MOCVD growth reactor. This problem can be encountered in the ICSP where a layer of GaAs is regrown over an etch-stop layer containing 10% of aluminum, or over a portion of p-clad material if there is no etch-stop layer. One approach to solving this problem is to chemically etch the region of the wafer slated for regrowth, then to bake the wafer in the reactor at high temperature (about 850°C) in a reducing atmosphere of hydrogen to remove the oxide, while using an over-pressure of arsine to prevent the evaporation of arsenic from the material. The amount of etch and the length of bake depend on the thickness of the native oxide. Excessive etch or prolonged baking time would remove too much material and destroy or dissolve the thin etch-stop and confining layers in the ICSP structure.

For the first experimental regrowth of ICSP lasers, we used our experience with DFB laser regrowth. Our DFB lasers were made by regrowth of material over a photolithography prepared grating. The grating fabrication process leaves impurities as well as native surface oxide, and a baking duration of about 30 minutes was found desirable in order to regrow successfully over it. Initially, the same assumption regarding impurities and native oxide was made for the ICSP, and upon testing the finished devices we found them to be non-lasing or to require large currents to operate, although ridge structures made from the same material had produced low threshold lasers. Microscopic examination of angled-

lap sections of the wafer indicated that the p-confining and the active layers had disappeared from the regrowth region.

We have learned that the pre-regrowth treatment of the ICSP wafers should not be as drastic as that for DFB lasers. In particular, although pre-bake is desired, its time duration should be much less than for DFB lasers because of the low aluminum content of the etch-stop layer. We have now successfully achieved the desired regrowth, and we have successfully tested several ICSP lasers.

### d. Results

Figure IV-7 shows the characteristics of two ICSP QW after regrowth. There are three important points to be noted in this data. The first and most important one is that the diodes were mounted in the junction up (p-up) configuration in a standard TO-46 package in order to test their thermal behavior. The second point is that the threshold current for this regrown structure is 15 mA, which is the same as for the ridge waveguides. The third point is that the diodes have linear characteristics well beyond 30 mW cw. These diodes exhibited single mode operation in both the longitudinal (Fabry-Perot) and spatial (waveguide) characteristics, and far-field radiation pattern of 9° by 34°. The p-up operation is possible because of the low threshold and low operating current (57 mA and 70 mA respectively for 30 mW cw). These diodes were driven to 100 mW cw in this p-up configuration, and their operation was kink-free (single mode) to beyond 50 mW cw.

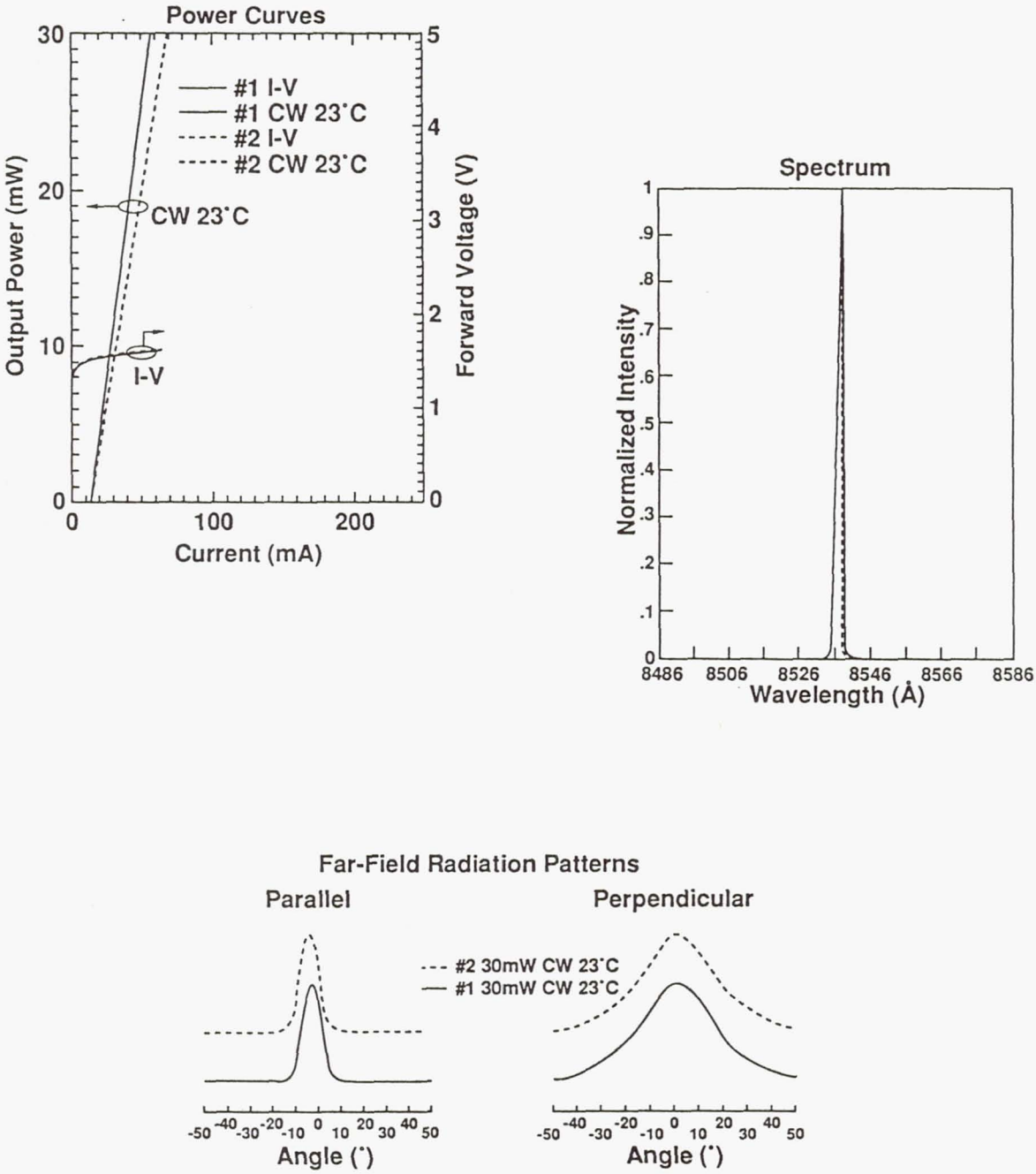


Figure IV-7. Light-current characteristics, spectra, and far-field radiation patterns of QW ICSP lasers.

## 2. LIFETEST AND DELIVERY OF ICSP LASERS

The mounted devices are tested using our automated characterization system. This system requires only the operator to load the package laser device into the system. The software is configured in a menu format to permit the operator to select whichever tests are required. The tests that were performed on the lasers, as specified in the contract, include P-I curves to 30 mW cw and 60 mW 50% duty cycle as well as parallel and perpendicular far-field radiation patterns at those power levels. In addition, the spectrum at the same power levels were taken. In Figs. IV-8 to 10, we show typical data plots before lifetesting for the P-I and I-V (Fig. IV-8), parallel and perpendicular far-field patterns and spectrum at a 30 mW cw level (Fig. IV-9), and parallel and perpendicular far-field patterns and spectrum at a 60 mW 50% duty-cycle (100 MHz) level (Fig. IV-10) for one of the ICSP laser devices. Similar data after 1577 hours are given in Figs. IV-11 to 13, respectively. The threshold current for the device is 15 mA with a slope efficiency of 44%. Both the pulse and cw P-I curves displayed linear behavior from threshold to the maximum power levels. The drive current at the 60 mW power level is about 115 mA. The far-field radiation patterns for both cw and pulse operation remain constant at about 36° and 9° for the perpendicular and parallel directions, respectively. The emission wavelength for the device was approximately 855 nm with only a single longitudinal mode evident in the cw spectrum.

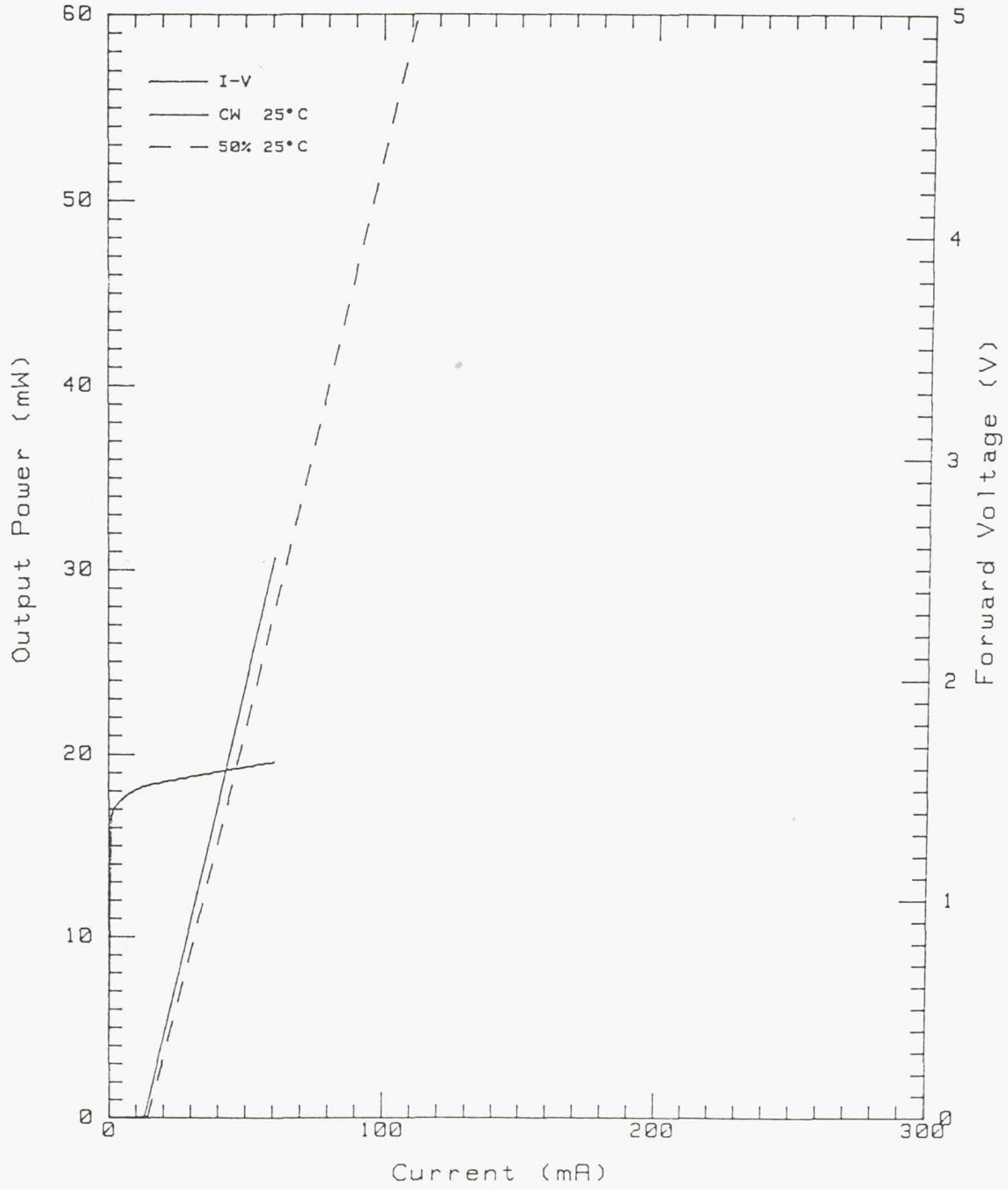


Figure IV-8. P-I characteristics of ICSP laser before lifetest.

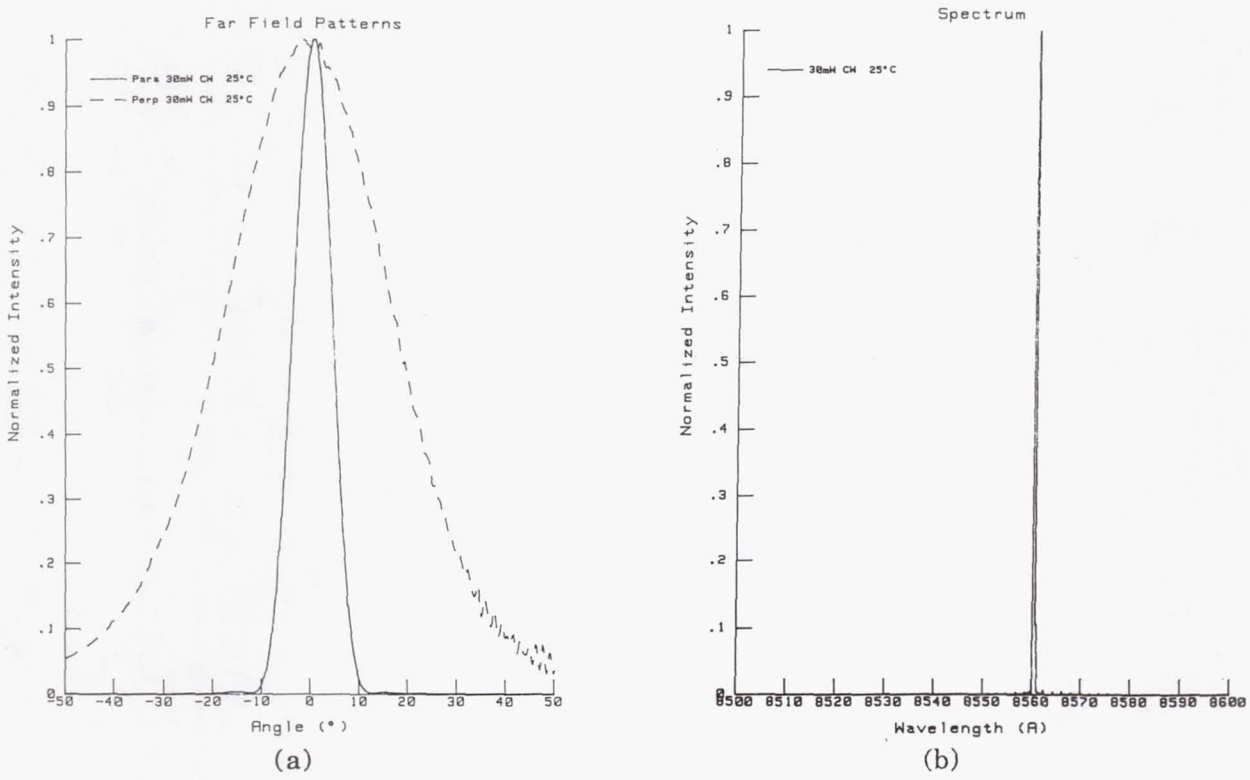


Figure IV-9. Far-field and output spectrum at 30 mW cw before lifetest.

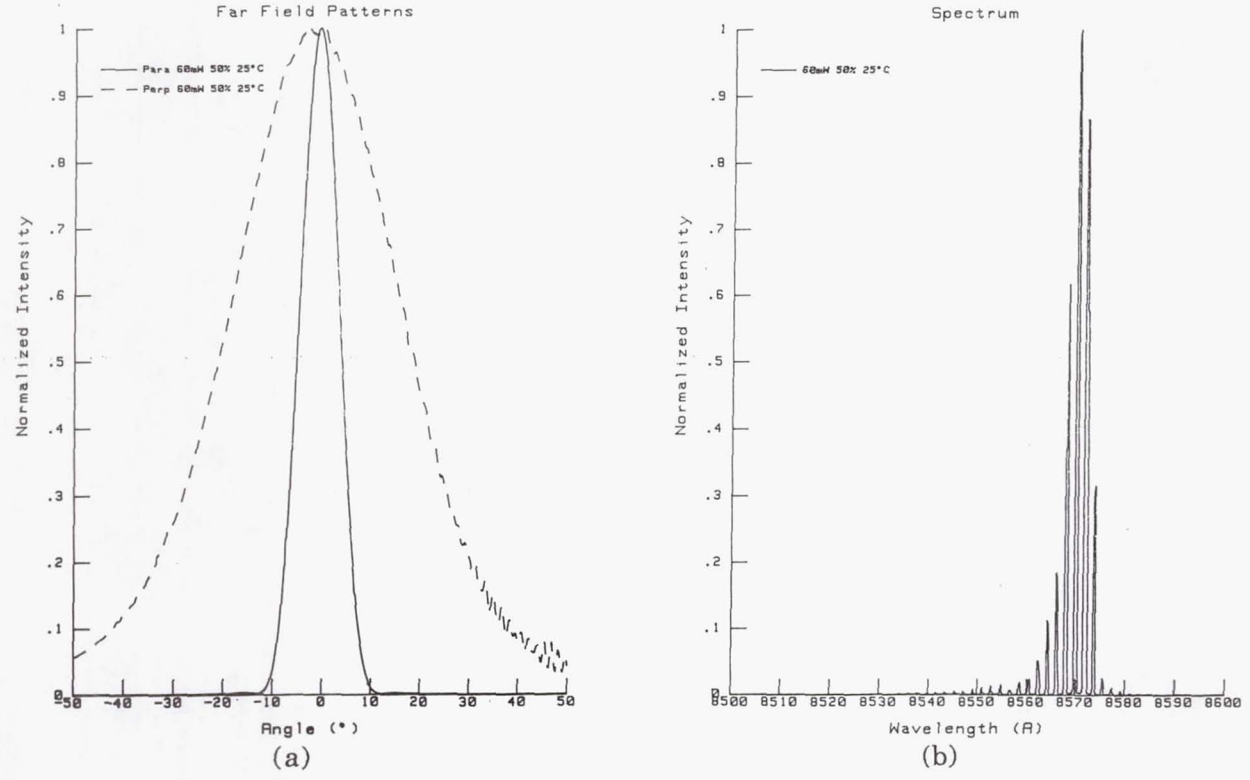


Figure IV-10. Far-field and output spectrum at 60 mW and 50% modulation at 100 MHz before lifetest.

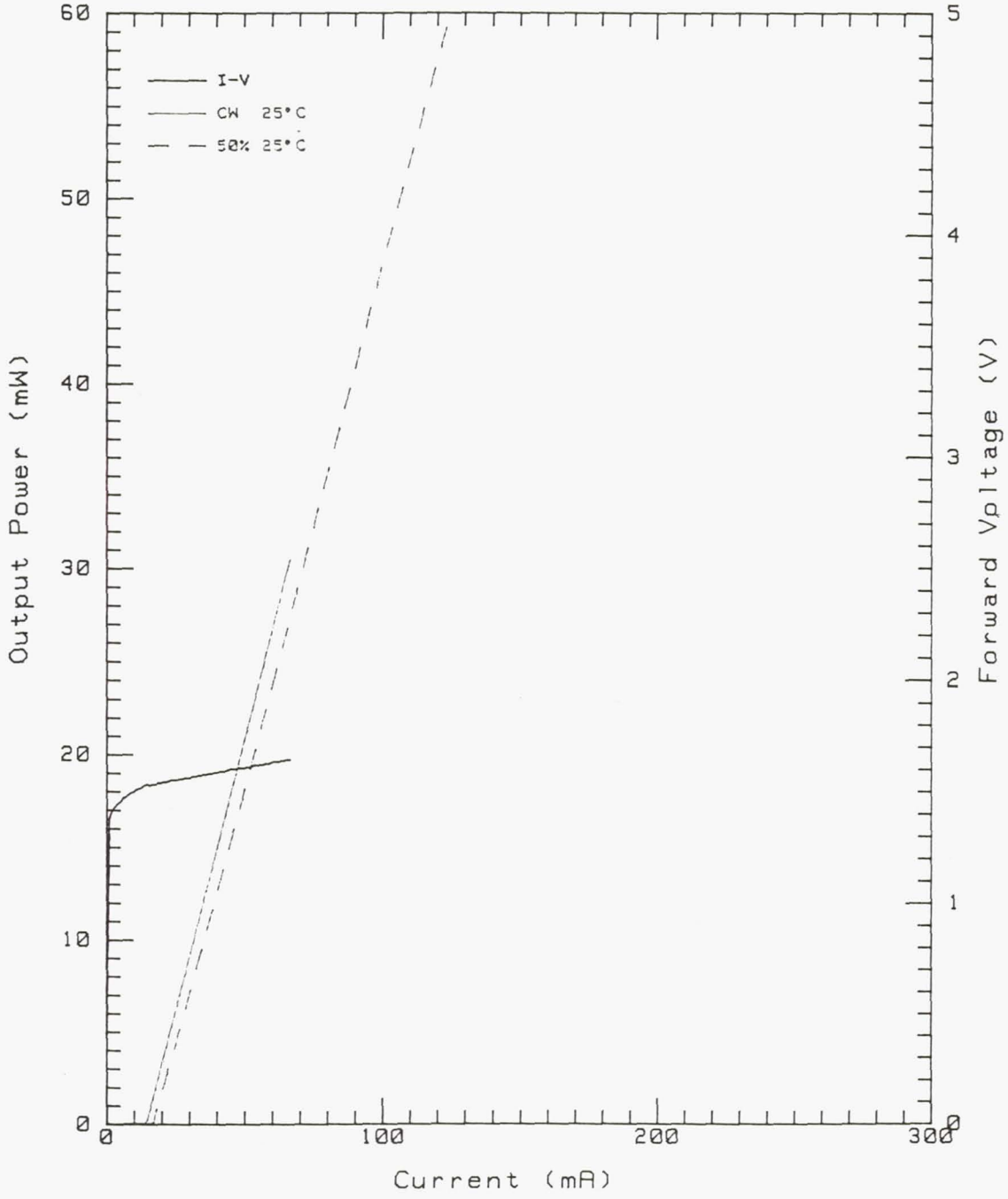


Figure IV-11. P-I characteristics of same laser after 1577 hour lifetest.

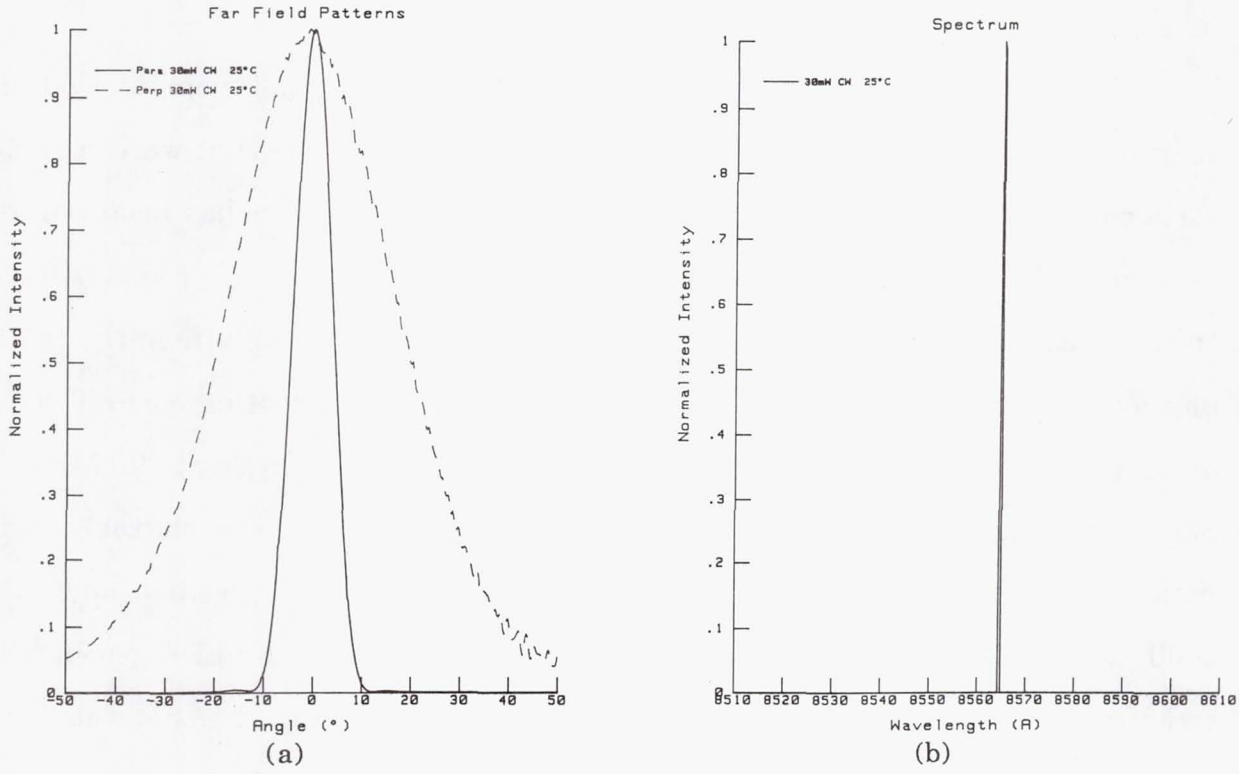


Figure IV-12. Far-field and output spectrum at 30 mW cw of same laser after 1577 hour lifetest.

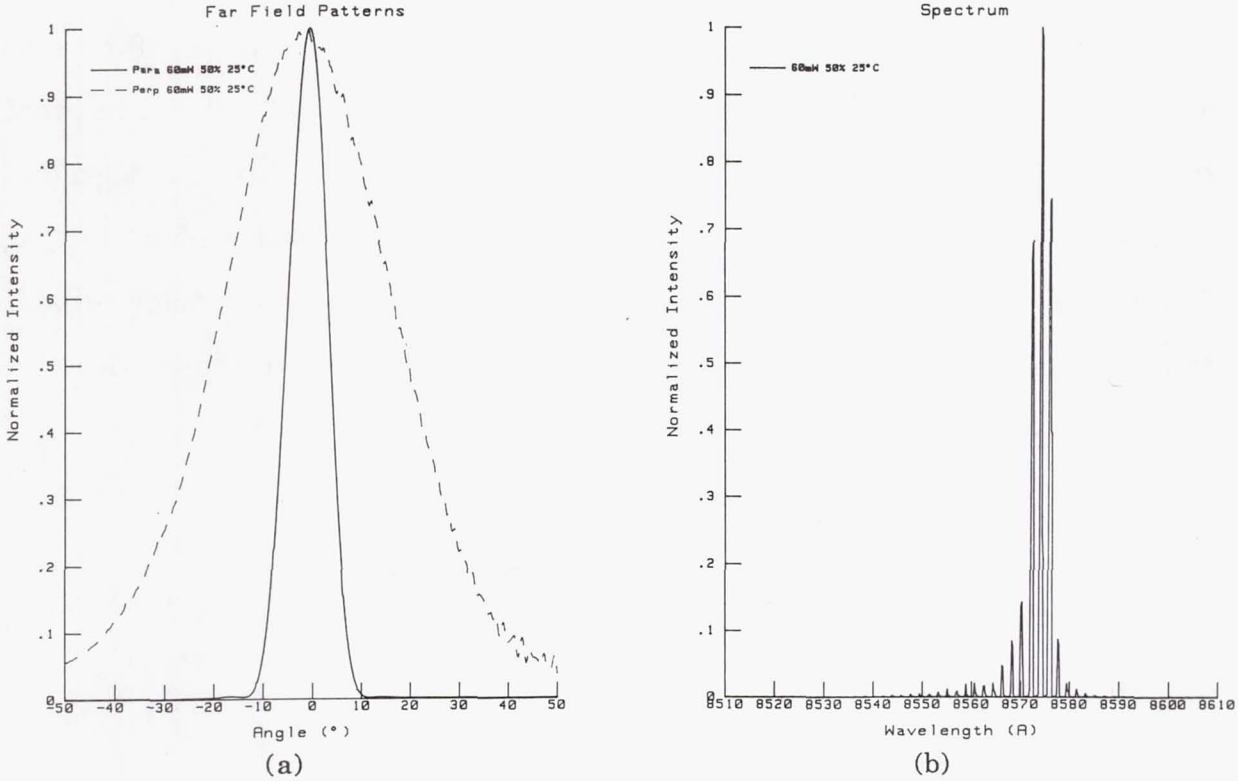


Figure IV-13 Far-field and output spectrum at 60 mW and 50% modulation at 100 MHz after 1577 hour lifetest.

The results presented here represent a significant improvement over the previous liquid phase epitaxial grown (LPE) CSP laser results that were reported earlier in this program. The threshold current for these devices has been reduced by a factor of three with an operational drive current at the 60 mW power level also greatly reduced. Both of these factors have contributed significantly to the improved reliability of this new structure. The results of lifetesting for four diodes under the full rated condition of 60 mW power and 50 % duty cycle at 100 MHz are plotted in Fig.IV-14. After an initial adjustment period, the characteristics remain essentially unchanged, staying well within contract specifications after 2000 hours. These results also indicate that changing from the LPE grown laser structure to a quantum well MOCVD laser structure during the contract was a sound engineering decision and was most appropriate given the previous results obtained with LPE prepared devices. This new MOCVD grown structure should provide NASA with a reliable, high-power AlGaAs laser device.

The contract deliverables for the program were shipped after a two-hundred hour burn-in evaluation at the 60 mW power level. They are proof of concept of the new laser structure. Only laser devices exhibiting no degradation through the burn-in evaluation period were selected for deliverables to NASA. The two-hundred hour time period was chosen based upon our prior reliability experience with the LPE CSP lasers and other MOCVD-grown laser devices.

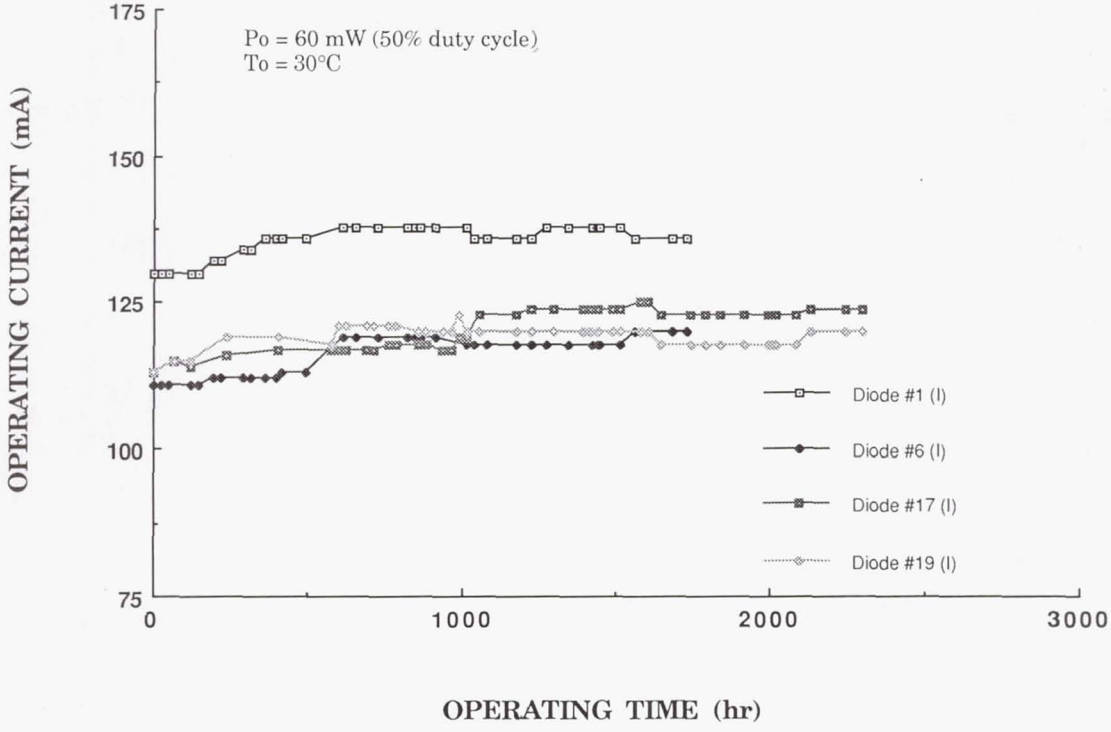


Figure IV-14. Output power vs time for four diodes under the full rated condition of 60 mW power and 50 % duty cycle at 100 MHz.

# Section V

# ANALYSIS OF DFB AND DBR LASER SOURCES FOR WAVELENGTH STABILITY

The ICSP lasers that were developed under this contract are Fabry-Perot types of devices. Their wavelength is strictly determined by the optical length of the laser cavity, which depends not only upon the physical length, but also upon injection current and temperature. More stable devices may be required for certain space applications. Such stability exists in DFB and DBR lasers in which a grating is used to stabilize the emission wavelength. The structures for DFB and DBR lasers are shown schematically in Fig. V-1a and Fig. V-1b respectively.

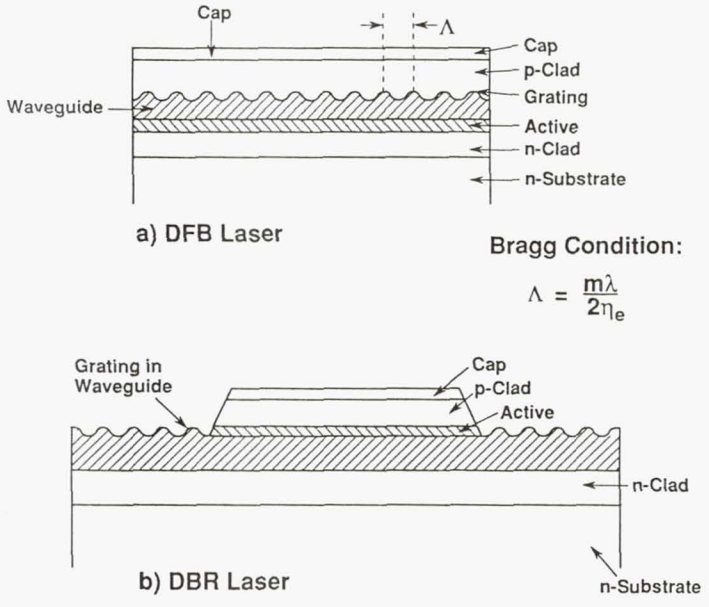


Figure V-1. (a) Structure of DFB laser. The grating is along the active region. (b) Structure of DBR laser. The gratings are placed in passive regions at the ends of the active region. They serve mainly as wavelength selective reflectors.

In the DFB laser, the grating is placed in a waveguide layer above (or below) the active layer. It interacts with the optical field in the active region, through the evanescent field in the waveguide, causing reflection of both forward and

backward waves. In the DBR laser, the grating is placed in passive waveguides in the end region, with the purpose of providing reflection feedback into the active region. Its function is thus similar to the facet in the F-P laser, except that the reflection is wavelength selective.

In this section, we report on the investigation of design and implementation strategies that lead to a choice between the two types of devices as sources for space communications systems. The features of interest in a laser are:

- Stable operation at one wavelength
- Immunity to mode hop
- Low RIN
- High power operation
- Long life, i.e., the avoidance of degradation mechanisms that may affect device life.

The features of both types of lasers will be examined in order to determine the preferred type.

## 1. DFB LASERS

### a. Modal Analysis

The operation of DFB lasers is readily derived from the theory of wave propagation in periodic structures. The grating introduces a periodic component in the permittivity of the waveguiding region. According to the Floquet-Block theorem for periodic differential equations, the wave propagating in the structure is also periodic, with the periodicity of the structure. A Fourier expansion decomposes it into a sum of its "partial" waves (harmonics). Pairs of these partial waves have matching phase in so-called "Bragg regions" where the grating period $\Lambda$ and the optical wavelength $\lambda$ are related by:

$$L = \frac{m\lambda_B}{2n_e} \qquad \text{(V-2)}$$

where m is an integer, and where the subscript $_B$ is added to identify the Bragg interaction. It is well known that energy exchange (or coupling) occurs between waves having matching phase, and in the case of the DFB laser, it occurs between a forward and backward wave harmonic.

Kogelnick and Shank [5] have used coupled-mode theory to derive the propagating modes and their threshold conditions in DFB structures. In a uniform waveguide, the wave amplitudes are constant with respect to longitudinal position z except for an attenuation factor if the guide is lossy. In the presence of a dielectric perturbation, $\Delta\mathcal{E}$, they become z-dependent, and if they are slowly varying, they are well described by coupled-mode theory. Near the Bragg region, the electric field, assumed to be polarized in the x direction and propagating in the z direction, is given by:

$$E(x,y,z) = u(x,y)\,[A(z)\exp(-j\beta_0 z) + B(z)\exp(j\beta_0 z)] \qquad \text{(V-3)}$$

where u(x,y) is the mode function (determined by guide geometry), where $\beta_0 = m\pi/\Lambda$ is the Bragg wavenumber, and where A(z) and B(z) are the coupled waves. It should be noted that Eq. V-3 is merely a representation of the field near the Bragg region. $\beta o$ is not the propagating wavenumber. The propagating wavenumber q is contained in the expressions for A(z), and B(z) which are given by:

$$A(z) = A_1 \exp(-jqz) + r(q)B_2 \exp(jqz),$$

$$B(z) = r(q)A_1 \exp(-jqz) + B_2 \exp(jqz) \qquad \text{(V-4)}$$

where $A_1$ and $B_2$ are constants, and r(q) is the DFB reflection coefficient, and where A(z) and B(z) obey the following coupled-mode equations:

$$\frac{dA}{dz} = -j\Delta\beta A - j\kappa B$$

$$\frac{-dA}{dz} = j\Delta\beta A - j\kappa A \qquad \text{(V-5)}$$

In the above expressions, $\Delta\beta = \beta - \beta_0$ is the phase mismatch, and $\beta$ is the complex propagation constant in the absence of the grating, given by:

$$\beta = n_e k_o + j\frac{1}{2}\bar{\alpha} \qquad \text{(V-6)}$$

as described earlier, and the coupling coefficient is given by:

$$\kappa = \frac{k_o^2}{2\beta} \frac{\int_{-\infty}^{\infty} \Delta\varepsilon u^2(x,y)dxdy}{\int_{-\infty}^{\infty} u^2(x,y)dxdy} \qquad \text{(V-7)}$$

The propagation constant q obeys the dispersion relation

$$q = \pm\left[(\Delta\beta)^2 - \kappa^2\right]^{1/2} \qquad \text{(V-8)}$$

and the DFB reflection coefficient r(q) is given by r(q) is given by:

$$r(q) = -\frac{\kappa}{q + \Delta\beta} \qquad \text{(V-9)}$$

The above treatment applies to a structure of infinite length, and expression V-8 gives the propagation constant. The waves propagate undisturbed as long as q is positive real. However, for $(\Delta\beta)^2 < \kappa^2$, q is pure imaginary and there is no propagation, i.e., there is a stop band of half-width equal to $\kappa$ centered at the Bragg wavenumbers. The longitudinal mode spectra and the threshold condition for the various modes are obtained when the finite length of the structure is taken into consideration.

**b. Threshold Condition**

For an infinitely long structure, q can have arbitrary values. For a finite length structure, the boundary conditions can be satisfied for only discrete values of q. For any value of q satisfying the boundary conditions to yield an output light with no input light (oscillation condition), the real part of q gives the longitudinal mode frequency, and its imaginary part gives the threshold gain. The DFB will lase at the frequency corresponding to the mode for which the threshold gain is the lowest. Then, if there is enough mode discrimination, only the mode with the lowest threshold will be favored for lasing.

For a finite length DFB, the effective facet reflectance is complex and its phase may be arbitrary, since the facet occurs at some arbitrary point in the grating. In general, they are given by:

$$r_1 = R_1^{1/2} \exp(-j\phi_1)$$

$$r_2 = R_2^{1/2} \exp(-j\phi_2) \qquad \text{(V-10)}$$

and the boundary conditions are, for a DFB of length L,

$$A(0) = r_1 B(0)$$

$$B(L) = r_2 A(L) \qquad \text{(V-11)}$$

Equations V-4 with boundary conditions (V-11) have a non-trivial solution only if the determinant of the coefficients vanishes, i.e., if the following resonance condition is satisfied.

$$\left(\frac{r_1 - r}{1 - rr_1}\right)\left(\frac{r_2 - r}{1 - rr_2}\right) \exp(-2jqL) = 1 \qquad \text{(V-12)}$$

Equation V-12 is the DFB laser eigenvalue equation and its numerical solution gives the longitudinal modes and their thresholds. Various effects can be

achieved by appropriate choices of $r_1$, $r_2$, and r (or $\kappa$). We note that this equation is reduced to the F-P threshold condition, $r_1 r_2 \exp(-2jqL) = 1$, if the coupling coefficient is zero, i.e., in the absence of the grating ($\kappa = 0$). Without going into mathematical details, we summarize the important results below when $\kappa$ is non-zero.

In the case of pure DFB operation, the facet reflections $r_1$ and $r_2$ are zero. Eq. V-12 gives $r^2 \exp(-2jqL) = 1$, which, together with (V-9) gives;

$$\kappa \sinh qL = \pm jq \qquad \text{(V-13)}$$

Equation V-13 can be solved graphically. The resulting DFB modes and their threshold gains are shown in Fig. V-2a. As expected, there is no propagating wave at the Bragg frequency. There are several modes symmetrically placed with respect to the Bragg frequency. The two modes closest to the Bragg frequency (heavy lines) have the lowest but equal threshold gain. Therefore the simple DFB laser with zero facet reflectance will lase in those two modes. Unlike the F-P laser for which the threshold gain is almost the same for a large number of modes, the DFB has a much higher threshold requirement for the modes that are further away from the Bragg frequency, and therefore, it has high selectivity. However, the existence of two modes is not desirable, and some means must be found to remove the degeneracy (remove one of the lasing modes).

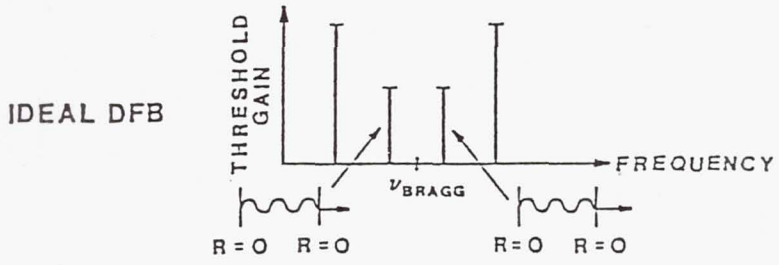


Figure V-2a. Ideal DFB has two modes with lowest threshold, identified by arrows.

One method consists of shifting the gain curve with respect to the DFB spectrum in order to give a lower threshold to one of the modes, as indicated in Fig. V-2b (the arrow points to be the selected line). This is not a desirable approach because the gain curve can vary with current, temperature, and age. Furthermore, it is very broad (about 150Å at the 3dB point for AlGaAs lasers), and therefore, this approach is unstable, and does not provide enough selectivity.

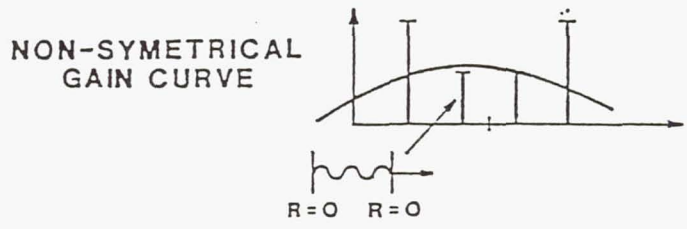


Figure V-2b. Shifting gain curve to select one mode.

Another method is to provide radiation losses for one of the degenerate modes. For example, if the grating is a second order grating m = 2 in Eq. V-2 instead of a first order grating, energy will be radiated out of the plane of the grating. Henry and Kazarinov have shown [6] that this loss is not the same for the modes on the two sides of the Bragg resonance, and hence, one of the modes will have a lower threshold, as shown in Fig. V-2c.

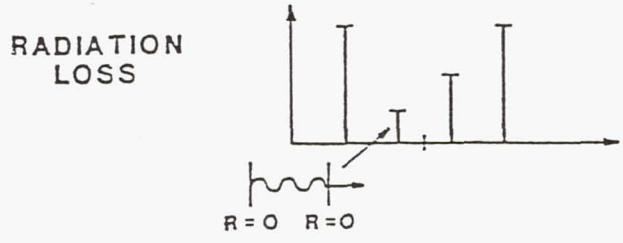


Figure V-2c. Use of radiation loss to select single mode.

Two other methods are shown for removing the DFB degeneracy, and their significance lies in the fact that they introduce a low gain threshold mode referred to as "gap mode", at the Bragg frequency itself. The first method is the introduction of a half-period (quarter wave) shift somewhere in the grating. This breaks the grating uniformity and introduces the equivalent of a half wavelength cavity that is resonant at the Bragg frequency. The effect of this scheme is to introduce a low threshold mode at the Bragg frequency. This type of structure is called the Quarter-Wave-Shifted (QWS) DFB laser. The second method is obtained from non-symmetrical facet reflection. It can be shown that if one of the facets has near unity reflectance and the other has near zero reflectance, a gap mode is also introduced in the spectrum. This structure is equivalent (as far as the modes are concerned) to a DFB with uncoated facets that is twice as long, and that has a shift in grating periodicity. In the case of a facet-coated DFB, the facet reflection will act as a grating phase shift, with the magnitude of the shift dependent on the position of the facet with respect to the grating. The gap mode in the DFB spectrum is shown in Fig. V-2d.

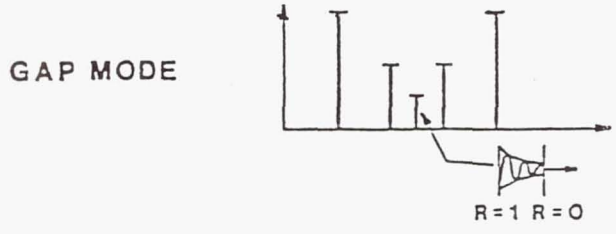


Figure V-2d. Creating low threshold "gap mode" at the Bragg wavelength.

The stronger the coupling coefficient $\kappa$ is, the lower is the required gain threshold. Figure V-3 shows the relation between the threshold gain coefficient and the coupling coefficient.

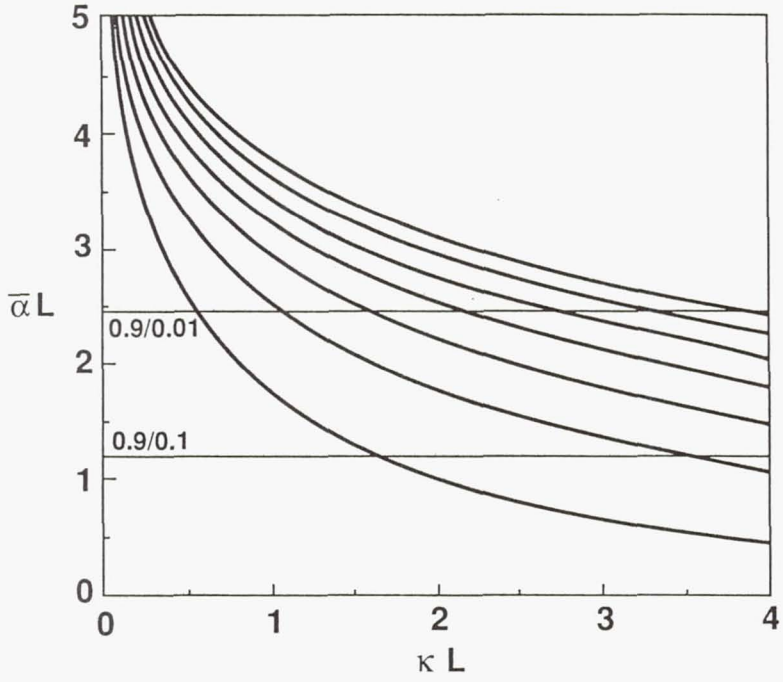


Figure V-3. Relation of threshold gain to coupling coefficient for DFB lasers.

It is therefore advantageous to have as strong a coupling coefficient as possible, but up to a certain point. However, if the grating is too strong, the spatial distribution of the modes becomes very non-uniform along the direction of propagation. This can result in multimode operation due to spatial hole burning. The coupling strength is a function of the grating corrugation depth, and a plot is given for a triangular grating in Fig. V-4.

## 2. DBR LASERS

In the DBR laser, the gain region is separated from the grating regions. The gratings are in passive waveguides at the ends of the device, and their purpose is to provide frequency selective reflectance as opposed to the broad-band facet reflectance of the F-P laser. The analysis of the grating reflection is also

given by coupled-mode theory, and the general solution is the same as Eq. V-4. If we denote the reflectance of the grating, referenced to the junction between the gain region and the grating by $r_g$, the threshold condition is given, for identical gratings, by

$$r_g^2 \exp(-j2\beta L) = 1 \qquad \text{(V-14)}$$

where $\beta$ is the same as before. If there are no transition discontinuity (between gain region and grating) or facet reflection,then $r_g$ is given by

$$r_g = \frac{j\kappa \sin(qL_g)}{q\cos(qL_g) + j\Delta\beta_g \sin(qL_g)} \qquad \text{(V-15)}$$

where $\Delta\beta_g = \delta - j\frac{1}{2}\alpha_g$, and where $\alpha_g$, is the grating power absorption coefficient.

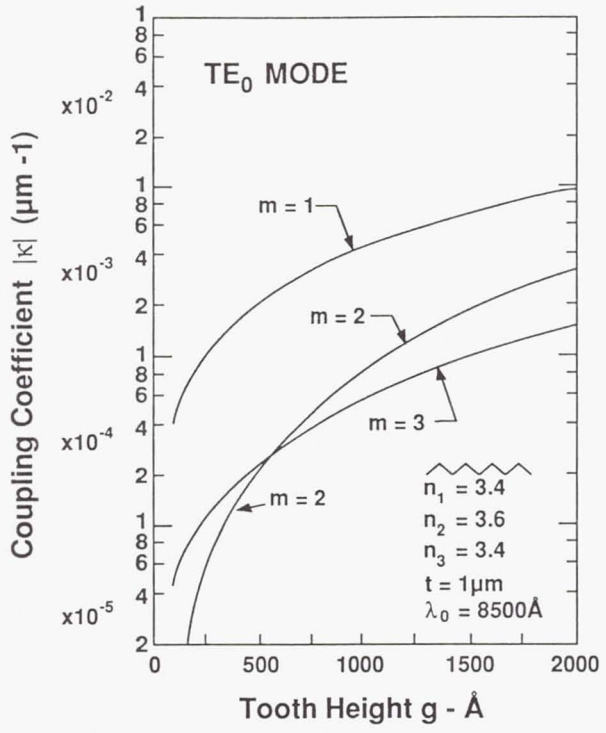


Figure V-4. Plot of coupling coefficient for triangular grating in DFB lasers.

DBR lasers do not have a stop band at the Bragg frequency. In fact, under ideal conditions, the mode of lowest gain threshold should occur at the Bragg frequency itself because this is where $r_g$ has its highest magnitude. However, because the feedback is not distributed within the gain region, the mode spectrum and oscillation conditions can vary, and they are significantly different than for a DFB laser. The mode frequencies are obtained by setting the phase of the left-hand side of Eq. V-14 to an integer multiple of $2\pi$. Once these eigen-frequencies are found, the required threshold gain is determined by setting to unity the amplitude of the left-hand side of Eq. V-14. It is thus clear that the actual wavelength of operation is critically sensitive to the phase length of the gain region. As operating conditions change (e.g. current, temperature), the wavelength of the various modes with respect to the Bragg resonance will change. Thus, it is possible that at one set of operating conditions one mode will be closest to the Bragg condition and will be favored to lase; if the conditions are changed, another mode will be favored. Therefore mode hopping is possible. However, despite this possibility for mode hopping, DBR lasers have been demonstrated to operate without mode hopping at output powers of several tens of milliwatts and over temperature variations of 50 to 70 °C.

## 3. CHOICE BETWEEN DFB AND DBR STRUCTURES

DBR lasers have the advantage that growth is not required over the grating region. It is well suited for optical integration because the grating can be designed to be both an output coupler and a coupling element to other devices, as in the GSE arrays under development at the David Sarnoff Research Center. With the addition of a long external cavity, it is an excellent structure for low chirp narrow linewidth sources. However, it has the disadvantage that mode stability

and selectivity depend on the phase length of the active region, on the length of the grating regions, and on the magnitude and phase of facet reflection. Furthermore, the transition between the active and grating regions may introduce significant radiation loss, which causes the lasing threshold to increase. Special waveguide transition is required to overcome radiation loss.

On the other hand, DFB lasers are real optical resonators that can have single mode operation over wide operating ranges. There is no waveguide transition to design, and the introduction of the QW shift, high facet reflectance on one side or longitudinal waveguide width variations can force the device to lase at exactly the Bragg wavelength with high selectivity and low threshold, regardless of operating conditions. This Bragg wavelength is determined strictly by the grating period and the waveguide's effective refractive index. In early DFB lasers, the grating was made in the active layer, and regrowth was required over that layer. Poor regrowth caused problems with device life, due to the introduction of non-radiative recombination centers. Later, the separate confinement structures solved the problem, because it allowed the fabrication of the grating in the confinement layer, which already protects the active layer. Finally TE/TM mode selectivity can be accomplished by facet reflection or, more importantly, by the use of QW active layers. For space applications, long life, high power, stable single mode operation, with low possibility of mode variations or hopping, are required. We conclude that DFB lasers are the most suitable type of stable source for space applications.

## 4. FIRST ORDER vs SECOND ORDER GRATING FOR DFB LASERS

Having shown that the DFB laser is suitable as a mode-stabilized source, we now examine the several issues that are involved in the design of such a source. The first issue is the laser geometry to be considered for inclusion of the DFB grating, with the condition that high power and low RIN are required in addition to modal stability. Since the active layer must be protected from the steps required to make the grating and regrow over it, the grating must be placed in a layer that functions both as a protective layer for the active layer and as a waveguide in which to place the grating. Therefore, a structure with separate confinement layers is desired. It can be a single QW, double QW, or even a double heterostructure with "thin" (400Å to 600 Å) active layer. The QW structures offer the advantage of giving control on the TE/TM polarization in favor of the TE mode. The structure must also provide adequate means for current and optical confinements. In that respect, gain-guided structures, are not desirable. Preferred structures are index-guided structures such as the ridge, buried ridge, and ICSP configurations. The ICSP DFB laser is an interesting choice because it provides the high power capability of the CSP without the alignment problems encountered in ordinary CSP lasers, due to its self-aligned geometry. It is also known to provide stable lateral guiding and high confinement characteristics.

The other important issue relates to the type of grating to be used. Fabrication of the grating should have a reasonable yield and should lend itself to inspection prior to regrowth. In addition, the grating design should facilitate mode selection, preferably by using a quarter-wave shift or a shift by reflection from the back facet. The grating is typically made by holographic exposure, using the 3511Å line of an argon laser on a photoresist layer spun on the wafer. The photoresist is then developed and the exposed lines are chemically etched.

the 3511Å line of an argon laser on a photoresist layer spun on the wafer. The photoresist is then developed and the exposed lines are chemically etched. Depending on the orientation of the grating lines, with respect to the crystal planes, two distinct grating shapes can be formed. If the grooves are aligned with respect to the (011) direction, a dovetail groove shape is obtained, and if the lines are aligned with respect to the $[0\bar{1}1]$ direction, a V-groove shape is obtained. Etching is carried both laterally and vertically. If it is allowed to proceed to completion, a triangular-shaped groove is obtained. If the etching is not complete, the shape of the groove is trapezoidal.

The simplest DFB structure is one that produces the Bragg condition in the first order (m = 1 in Eq. VI-2), with the grating period equal to half wavelength in the guide. For a 8300 Å laser with a AlGaAs waveguide having a refractive index of 3.4, the grating period is 1220 Å. Such a grating is very difficult to fabricate and, it cannot be inspected with visible light. Furthermore, the grating depth, hence, the DFB coupling coefficient, cannot be easily controlled. The fabrication difficulty is enhanced by the fact that a quarter-wave shift may be desired in order to operate at the Bragg wavelength for single mode performance.

Several methods have been used or proposed to fabricate gratings of period in the 1000 Å range in III-V compounds. The most feasible method appears to be the "divide-by-two", and we describe three of these here. The first method is illustrated in Fig. V-5. A grating of period equal to twice the desired period is fabricated on the substrate using conventional holographic and photoresist techniques, then it is covered with a dielectric, such as silicon nitride, as shown in Fig. V-5a. The dielectric is ion milled to expose the grating crests, as shown in Fig. V-5b, and a second grating with the same period is fabricated on the material with a half-period shift as shown in Fig. V-5c. The shift can be obtained either by inserting a half-wave plate in one of the holographic beams, or by mounting one of

the mirrors on a PZT element to which a voltage is applied to create a half-wave displacement. The final grating is obtained after removal of the residual dielectric.

A second method is shown in Fig. V-6. According to this technique, the first grating is exposed as before, as shown in Fig. V-6a, but it is not etched. Instead, it is covered with a nitride film (Fig. V-6b) on which a second holographic exposure is done, as shown in Fig. V-6c. The dual pattern is then etched to produce the desired grating (Fig. V-6d).

A third method for the divide-by-two approach is shown in Fig. V-7. In this case, a rectangular grating is formed in the resist, and a conformal dielectric coating is deposited, as shown in Fig. V-7b. This is followed by an ion beam etch at grazing incidence to expose the top of the photoresist as shown in Fig. V-7c. The resist is then dissolved (Fig. V-7d) and the substrate is ion beam etched (Fig. V-7e). The finished grating is obtained after removal of the residual oxide mask (Fig. V-7f).

The other techniques used for making high-pitch gratings include direct E-beam writing, the use of short wavelength lasers, the use of high index prisms, immersion in high index fluid, the use of cross gratings, and the use of focussed ion beam etching. These methods and their relative merits are summarized in Table V-1.

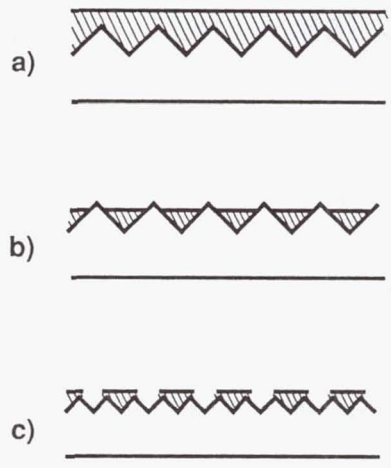


Figure V-5. A "divide-by-two" method to produce grating with period in the 1000Å range.

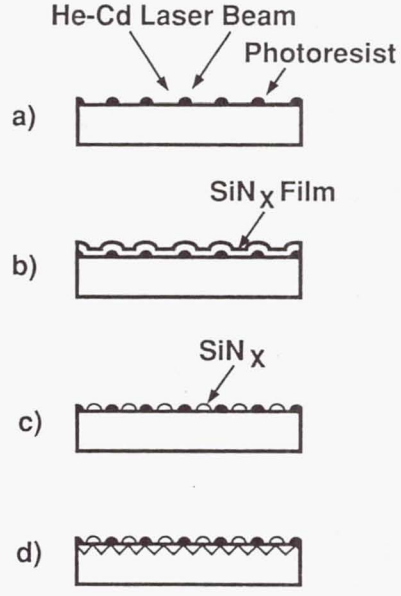


*Fabrication steps of 120 nm period grating.*

a. Holographic exposure
b. $SiN_x$ deposition by ECR-CVD
c. Etch $SiN_x$ with BHF
d. Etch substrate

Figure V-6. Alternative method to produce short period gratings (details in text).

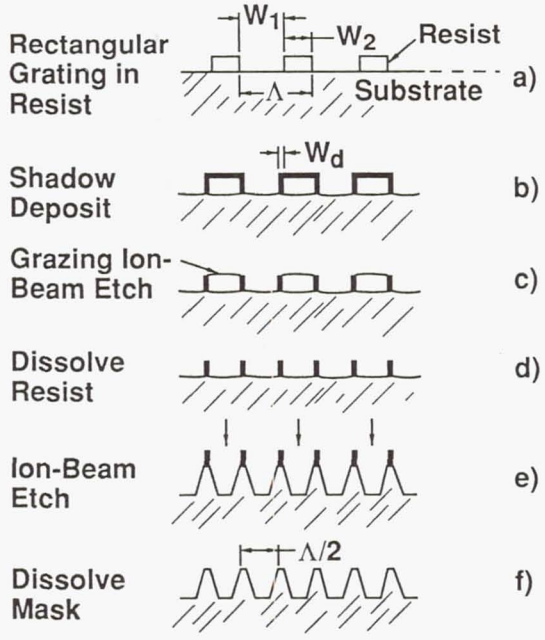


Figure V-7. Third method for producing short period gratings.

## Table V-1
## Grating Fabrication Methods For Λ ~ 1000Å

| CONCEPT | MIN | COMMENTS |
|---|---|---|
| 1. DIVIDE BY 2 | ~878 Å (Ar)<br>~813 Å (HeCd) | QUESTIONABLE REPRODUCIBILITY |
| 2. E-BEAM WRITING | ~1000 Å | ~1 mm x 1 mm FIELD; TIME CONSUMING<br>1/4-WAVE SHIFT EASY, $1000 K |
| 3. SHORT WAVELENGTH LASERS | | |
| – XENON | λ = 2315 Å | ~1 mm x 1 mm FIELD; NON-COMMERCIAL LASER |
| – ArF, | λ = 965 Å | COHERENCE? FIELD? PMMA, $60K; PULSED |
| 4. HIGH INDEX PRISM n ~ 1.7 | ~1157 Å (Ar)<br>~1161 Å (HeCd) | REQUIRES PLANAR WAFER; $5K |
| 5. IMMERSION IN HIGH INDEX FLUID n ~ 1.4 | ~1254 Å (Ar) | FLUID COMPATIBILITY; > 1000 Å, $10K |
| 6. CROSS GRATING | < 1000 Å | LATERAL SCATTERING; EXISTING CAPABILITY |
| 7. FOCUSSED ION BEAM ETCHING | ~ 1000 Å | NOT DEMONSTRATED; $500 K<br>140 μM X 140 μM FIELD<br>1/4 WAVE SHIFT EASY |

As can be seen from the above discussion, the fabrication of a first order sinusoidal grating for a 830 nm DFB laser (grating period of 1200 Å) is not an easy task. However, a non-sinusoidal grating can be designed to have a strong harmonic component in any specific order. For example, a grating can be designed to have a fundamental wavelength of 2400 Å with a strong component at 1200 Å (second harmonic). Such a grating, designed to operate at the second harmonic is called a "second order" grating, and a DFB laser containing it would have a strong response at the second Bragg condition, i.e., the condition corresponding to m = 2 in Eq.V-2. It is also easier to fabricate than a "first order" grating, i.e., one for which m = 1, because the grating spacing is twice as large as that for the first order grating. The second order grating is also desirable because it can be used to enhance mode selection. The basic idea here is to use available techniques of holography and chemical photolithography, perhaps enhanced by ion beam etching to create a non-sinusoidal grating of suitable shape to enhance the second harmonic. Figure V-8 illustrates some grating shapes that are suitable for second order coupling and others that are not. The rectangular grating can be made to have a relatively strong second harmonic component.

Since the coupling coefficient is proportional to the amplitude of the respective component of waveguide permittivity perturbation, the magnitude of the grating's second harmonic Fourier coefficient is thus a measure of the coupling coefficient in that order. The second order coupling strength of several gratings is given in Table V-2.

We see that a rectangular grating with 25% duty factor has a second order coupling strength of 60% of the first order coupling strength. It can be made by a combination of chemical and ion beam etchings. The above analysis concludes our preliminary study of DFB and DBR lasers for space applications. Several options have been examined and our preferred choices are described. We

recommend the fabrication of DFB lasers using a second order grating embedded in the confinement layer above the active layer, in an index-guided structure, such as the ICSP, that provide both current and optical confinement.

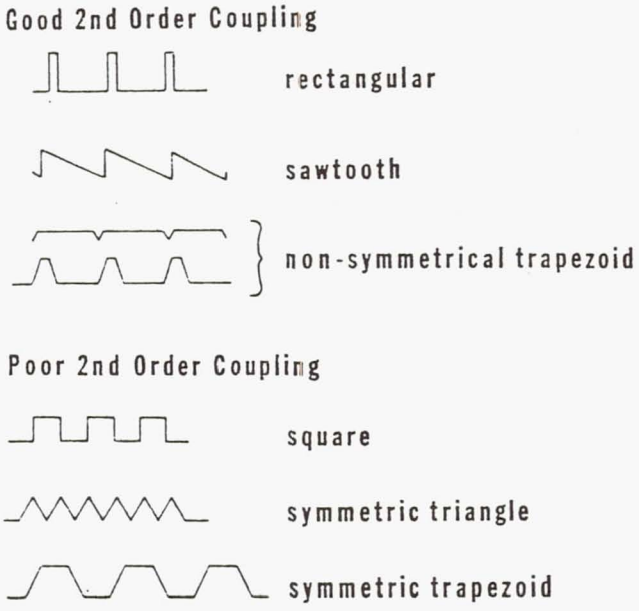


Figure V-8 Grating shape categorized as good and poor for second order DFB laser.

**Table V-2**

**COMPARISON OF 1st AND 2nd BRAGG REFLECTORS**

| Grating Shape | Order | Relative κ |
|---|---|---|
| Sinusoidal | 1 | 1 |
| sinusoidal | 2 | 0.01 to 0.1 |
| Rectangular (25% d.c.) | 2 | 0.6 |
| Sawtooth | 2 | 0.3 |
| Triangular | 2 | 0.01 to 0.1 |
| half-sine | 2 | 0.4 |

# Section VI

# CONCLUSIONS

The continued support of the high-power CSP laser by NASA has led to an increased understanding of it's operational characteristics and has led to substantial developments in computer modeling, liquid phase epitaxial growth and processing procedures. In addition, this support has identified the reliability limitations associated with the CSP laser structure and the development of the new ICSP laser which has demonstrated improved reliability at high operational powers compared with the CSP laser. The development of the ICSP laser grown by MOCVD techniques has led to the desired 1-2 mW/Khr degradation rate for lifetest lasers at 60 mW of optical power. This result coupled with the improved operational characteristics of the ICSP laser makes this device a superior candidate for space communication systems.

The results from the theoretical study of DFB- and DBR-type lasers has identified the DFB laser as the laser structure most suitable for coherent space communication systems requiring single frequency operation. Further, the study has shown that second-order Bragg gratings can be fabricated, which will provide strong optical feedback for single-frequency operational during high-speed modulation.

# REFERENCES


1. J. J. Hsieh, "Thickness and surface morphology of GaAs LPE layers grown by supercooling, step-cooling, equilibrium-cooling, and two-phase solution techniques," J. Crystal Growth 27 (1974) 49.

2. Ibid.

3. D. Botez, W. Tsang, and S. Wang, "Growth characteristics ofGaAs-$Ga_{1-x}Al_xAs$ structures fabricated by liquid-phase epitaxy over preferentially etched channels," Appl. Phys. Lett. 28 (1976) 234.

4. T. Murakami, K. Ohtaki, H. Matsubara, T. Yamawaki, H. Saito, K. Isshiki, Y. Kokubo, A. Shima, H. Kumabe, and W. Susaki, "A very narrow-beam AlGaAs laser with a thin tapered-thickness active layer ($T^3$ laser)," IEEE J. Quantum Electron., QE-23 (1987) 712.

5. H. Kogelnik and C.V. Shank, "Coupled-Wave Theory of Distributed Feedback Lasers," J. Appl. Phys, 43, 2327 (1972).

6. R. F. Kazarinov, and C. H. Henry, "Second-Order Distributed Feedback lasers with Mode Selection Provided by First-Order Radiation Losses," IEEE J. Quantum Electron. QE-21, 144 (1985).

NASA
National Aeronautics and Space Administration

# Report Documentation Page

| 1. Report No. | 2. Government Accession No. | 3. Recipient's Catalog No. |
|---|---|---|
| NASA CR-4345 | | |

| 4. Title and Subtitle | 5. Report Date |
|---|---|
| Improving the Reliability and Modal Stability of High Power 870 nm AlGaAs CSP Laser Diodes for Applications to Free Space Communication Systems | March 1991 |
| | 6. Performing Organization Code |

| 7. Author(s) | 8. Performing Organization Report No. |
|---|---|
| J. C. Connolly, G. A. Alphonse, D. B. Carlin, and M. Ettenberg | |
| | 10. Work Unit No. 506-44-21-01 |

| 9. Performing Organization Name and Address | 11. Contract or Grant No. |
|---|---|
| David Sarnoff Research Center<br>Princeton, NJ 08543-5300 | NAS1-18226 |
| | 13. Type of Report and Period Covered |
| 12. Sponsoring Agency Name and Address | Contractor Report |
| National Aeronautics and Space Administration<br>Langley Research Center<br>Hampton, VA 23665-5225 | 14. Sponsoring Agency Code |

15. Supplementary Notes

Langley Technical Monitor: Herbert D. Hendricks
Final Report - Task 6

16. Abstract

The operating characteristics (power-current, beam divergence, etc.) and reliability assessment of high-power CSP lasers is discussed. The emission wavelength of these lasers has been optimized at 860-880 nm. The operational characteristics of a new laser, the inverse channel substrate planar (ICSP) laser, grown by metalorganic chemical vapor deposition (MOCVD), is discussed and the reliability assessment of this laser is reported. The highlights of this study include a reduction in the threshold current value for the laser to 15 mA and a degradation rate <2 KW/hr for the lasers operating at 60 mW of peak output power.

| 17. Key Words (Suggested by Author(s)) | 18. Distribution Statement |
|---|---|
| Semiconductor Laser<br>High Power<br>AlGaAs (Aluminum Gallium Arsenide)<br>Index Guided | Unclassified - Unlimited<br>Subject Category 36 |

| 19. Security Classif. (of this report) | 20. Security Classif. (of this page) | 21. No. of pages | 22. Price |
|---|---|---|---|
| UNCLASSIFIED | UNCLASSIFIED | 88 | A05 |

NASA FORM 1626 OCT 86

For sale by the National Technical Information Service, Springfield, Virginia 22161-2171

NASA-Langley, 1991